

AD-A166 429

AFWAL-TR-85-4093

CRACK GROWTH IN TITANIUM ALLOYS UNDER
THE CONJOINT ACTION OF HIGH AND LOW
CYCLE FATIGUE



DTIC
ELECTE
APR 09 1986
S D

G. E. Powell and I. Henderson
Mechanical Behaviour of Materials
Department of Mechanical Engineering
Portsmouth Polytechnic
Anglesea Road, Portsmouth
Hampshire PO1 3DJ England

February 1986

Final Report for Period June 1983 - June 1985

Approved for public release; distribution unlimited

MATERIALS LABORATORY
AIR FORCE WRIGHT AERONAUTICAL LABORATORIES
AIR FORCE SYSTEMS COMMAND
WRIGHT-PATTERSON AIR FORCE BASE, OHIO 45433-6533

and

EUROPEAN OFFICE OF AEROSPACE RESEARCH AND DEVELOPMENT
LONDON, ENGLAND

DTIC FILE COPY


86 4 8 038

NOTICE

When Government drawings, specifications, or other data are used for any purpose other than in connection with a definitely related Government procurement operation, the United States Government thereby incurs no responsibility nor any obligation whatsoever; and the fact that the government may have formulated, furnished, or in any way supplied the said drawings, specifications, or other data, is not to be regarded by implication or otherwise as in any manner licensing the holder or any other person or corporation, or conveying any rights or permission to manufacture use, or sell any patented invention that may in any way be related thereto.

This report has been reviewed by the Office of Public Affairs (ASD/PA) and is releasable to the National Technical Information Service (NTIS). At NTIS, it will be available to the general public, including foreign nations.

This technical report has been reviewed and is approved for publication.

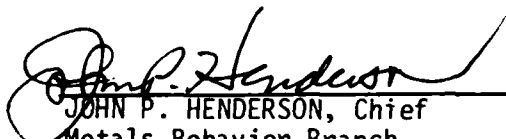


DAVID I.G. JONES, Mat'l's Rsch Engr
Metals Behavior Branch
Metals and Ceramics Division
Materials Laboratory



ALLAN W. GUNDERSON, Tech Area Mgr
Metals Behavior Branch
Metals and Ceramics Division
Materials Laboratory

FOR THE COMMANDER



JOHN P. HENDERSON, Chief
Metals Behavior Branch
Metals and Ceramics Division
Materials Laboratory

"If your address has changed, if you wish to be removed from our mailing list, or if the addressee is no longer employed by your organization please notify AFWAL/MLLN, W-PAFB, OH 45433 to help us maintain a current mailing list".

Copies of this report should not be returned unless return is required by security considerations, contractual obligations, or notice on a specific document.

UNCLASSIFIED

SECURITY CLASSIFICATION OF THIS PAGE

REPORT DOCUMENTATION PAGE

1a. REPORT SECURITY CLASSIFICATION UNCLASSIFIED			1b. RESTRICTIVE MARKINGS		
2a. SECURITY CLASSIFICATION AUTHORITY			3. DISTRIBUTION/AVAILABILITY OF REPORT Approved for public release; distribution unlimited.		
2b. DECLASSIFICATION/DOWNGRADING SCHEDULE					
4. PERFORMING ORGANIZATION REPORT NUMBER(S)			5. MONITORING ORGANIZATION REPORT NUMBER(S) AFWAL-TR-85-4093		
6a. NAME OF PERFORMING ORGANIZATION Mechanical Behaviour of Materials		6b. OFFICE SYMBOL (If applicable)	7a. NAME OF MONITORING ORGANIZATION Air Force Office of Scientific Research (AFOSR)		
6c. ADDRESS (City, State and ZIP Code) Portsmouth Polytechnic Hants PO1 3DJ England			7b. ADDRESS (City, State and ZIP Code) Bolling AFB Washington DC 20332		
8a. NAME OF FUNDING/SPONSORING ORGANIZATION Materials Laboratory		8b. OFFICE SYMBOL (If applicable) AFWAL/MLLN	9. PROCUREMENT INSTRUMENT IDENTIFICATION NUMBER F49620-83-C-0116DEF		
8c. ADDRESS (City, State and ZIP Code) AF Wright Aeronautical Laboratories, AFSC Wright-Patterson Air Force Base OH 45433-6533			10. SOURCE OF FUNDING NOS.		
			PROGRAM ELEMENT NO. 61102	PROJECT NO. 2420	TASK NO. 01
					WORK UNIT NO. 50
11. TITLE (Include Security Classification) Crack Growth in Ti Alloys (Unclassified)					
12. PERSONAL AUTHOR(S) B. E. Powell and I. Henderson					
13a. TYPE OF REPORT Final Report		13b. TIME COVERED FROM 15Jun83 TO 14Jun85		14. DATE OF REPORT (Yr., Mo., Day) February 1986	
				15. PAGE COUNT 77	
16. SUPPLEMENTARY NOTATION					
17. COSATI CODES			18. SUBJECT TERMS (Continue on reverse if necessary and identify by block number)		
FIELD	GROUP	SUB. GR.	RFC		
			Fatigue Crack Growth Minor Cycles da/dN Data		
			Dual Frequency Loading Fatigue Thresholds Ti-6Al-4V		
			Low/High Cycle Fatigue Major-Minor Cycling Ti-5331S		
19. ABSTRACT (Continue on reverse if necessary and identify by block number) Fatigue crack propagation rates have been measured for two titanium-based aeroengine disc alloys using compact tension test pieces. The loading block employed simulates two features of the engine flight pattern. A major stress cycle represents the start-stop operation which leads to low cycle fatigue. In-flight vibrations, which may give rise to high cycle fatigue, are represented by superimposed minor cycles of high frequency. With a lifing policy of retirement for cause the useful lives of blades and discs are limited by the onset of minor cycle crack growth. The threshold values associated with the minor cycles have been used to predict this event. Similarly the method of linear summation has been used to predict the subsequent fatigue crack growth rates. These predictions are successful for Ti-6Al-4V, whilst for Ti-5331S they are found to be either accurate or safe. Although Ti-5331S displays a marginally greater resistance to the onset of minor cycle crack growth, of greater significance is its reduced crack growth rates prior to this event. As a consequence components fabricated from Ti-5331S will exhibit longer fatigue crack propagation lives when subjected to the conjoint action of high and low cycle fatigue.					
20. DISTRIBUTION/AVAILABILITY OF ABSTRACT UNCLASSIFIED/UNLIMITED <input checked="" type="checkbox"/> SAME AS RPT. <input type="checkbox"/> DTIC USERS <input type="checkbox"/>			21. ABSTRACT SECURITY CLASSIFICATION Unclassified		
22a. NAME OF RESPONSIBLE INDIVIDUAL Dr D.I.G. Jones			22b. TELEPHONE NUMBER (Include Area Code) 513-255-2689		22c. OFFICE SYMBOL AFWAL/MLLN

FOREWORD

This report was prepared by the Mechanical Behaviour of Materials Laboratory, Portsmouth Polytechnic, England, for the Metals Behavior Branch, Metals and Ceramics Division, Materials Laboratory, Air Force Wright Aeronautical Laboratories (AFWAL/MLLN), under contract No. F49620-83-C-00116DEF, Program Element 61102, Project No. 2420, Task No. 01, Work Unit No. 50. The work was administered under the direction of Dr D. Jones, through the Air Force Office of Scientific Research (AFOSR), Bolling AFB, Washington DC and the European Office of Aerospace Research (AFOSR), London, England. The investigation was conducted at the Mechanical Behaviour of Materials Laboratory, under the leadership of Prof T. V. Duggan, and the experimental study was accomplished by B. E. Powell and I. Henderson. This report describes work conducted from 15 June 1983 through 14 June 1985.

The authors wish to acknowledge the support received from the Metals Behavior Branch, Wright-Patterson AFB, Ohio; Rolls-Royce, Derby; and Portsmouth Polytechnic. We also wish to record our thanks to those of our colleagues who have contributed to this study in any way.



Accession For	
NTIS	CRA&I <input checked="" type="checkbox"/>
DTIC	TAB <input type="checkbox"/>
Unannounced <input type="checkbox"/>	
Justification	
By	
Distribution /	
Availability Codes	
Dist	Avail and/or Special
A-1	

TABLE OF CONTENTS

SECTION	PAGE
1. INTRODUCTION	1
2. OBJECTIVES AND APPROACH	3
3. CRACK GROWTH IN Ti-6Al-4V	5
3.1 EFFECT OF AMPLITUDE AND CYCLE RATIO	5
3.2 THE ONSET OF MINOR CYCLE ACTIVITY	5
3.3 PREDICTING FATIGUE CRACK GROWTH RATES	9
3.4 A LOW VIBRATIONAL AMPLITUDE	9
3.5 THE EFFECT OF REST PERIODS	12
4. CRACK GROWTH IN Ti-5331S	14
4.1 INTRODUCTION	14
4.2 LOW CYCLE FATIGUE CRACK GROWTH	14
4.3 HIGH CYCLE FATIGUE CRACK GROWTH	16
4.4 CRACK GROWTH UNDER COMBINED LOW AND HIGH CYCLE FATIGUE	16
5. CRACK CLOSURE	25
6. FRACTOGRAPHIC STUDIES	36
6.1 INTRODUCTION	36
6.2 FATIGUE CRACKING PROCESSES IN Ti-6Al-4V	36
6.3 FATIGUE CRACKING PROCESSES IN Ti-5331S	41
7. DISCUSSION	48
7.1 INTRODUCTION	48
7.2 THE ROLE OF CRACK CLOSURE	48
7.3 THE ONSET OF MINOR CYCLE ACTIVITY	48
7.4 CRACK GROWTH WITH ACTIVE MINOR CYCLES	52

TABLE OF CONTENTS (CONTINUED)

	PAGE
7.5 FRACTURE MECHANISMS	53
7.6 CONCLUDING REMARKS	57
8. CONCLUSIONS	58
REFERENCES	60
LIST OF SYMBOLS AND ABBREVIATIONS	66

LIST OF ILLUSTRATIONS

FIGURE	PAGE
1. Load sequences: (a) major cycle only, (b) minor cycles superimposed on the dwell period of the major cycle.	2
2. Effect of amplitude ratio. Data for Ti-6Al-4V and a cycle ratio of 10 000.	6
3. Effect of cycle ratio. Data for Ti-6Al-4V and an amplitude ratio of 0.12.	7
4. Near-threshold FCG data for Ti-6Al-4V at a stress ratio of 0.82.	10
5. FCG rates in Ti-6Al-4V at an amplitude ratio of 0.22 and a cycle ratio of 1000.	11
6. Effect of rest period. Data for Ti-6Al-4V at an amplitude ratio of 0.32 and a cycle ratio of 1000.	13
7. Major cycle FCG rates for Ti-6Al-4V and Ti-5331S at a stress ratio of 0.1.	15
8. Comparison of major cycle FCG rates for Ti-5331S.	17
9. Near-threshold FCG data for Ti-5331S at a stress ratio of 0.80-0.82.	18
10. Near-threshold FCG data for Ti-5331S at a stress ratio of 0.90.	19
11. FCG rates in Ti-5331S at an amplitude ratio of 0.12 and a cycle ratio of 10 000.	21
12. FCG rates in Ti-5331S at an amplitude ratio of 0.22 and a cycle ratio of 10 000.	22
13. Sequence of load versus BFS traces at progressively greater crack lengths.	26
14. Crack closure behaviour in Ti-5331S for major cycle only loading.	28
15. Crack closure behaviour in Ti-5331S for $Q = 0.22$ and $n = 10\ 000$.	29
16. Crack closure behaviour in Ti-6Al-4V: (a) $Q = 0.33$ and $n = 1000$, (b) $Q = 0.32$ and $n = 1000$.	30

LIST OF ILLUSTRATIONS (CONTINUED)

	PAGE
17. Crack closure behaviour in Ti-6Al-4V: (a) $Q = 0.22$ and $n = 10\ 000$, (b) $Q = 0.12$ and $n = 100\ 000$.	31
18. Correlation of FCG rates with ΔK_{eff} for two titanium alloys.	32
19. Schematic of dynamic closure monitoring system: (a) load versus BFS trace, (b) load versus compensated BFS trace.	33
20. Absence of crack closure in high frequency minor cycles: (a) load versus BFS trace, (b) load versus compensated BFS trace.	34
21. Major cycle crack growth in Ti-6Al-4V by cyclic cleavage and ductile striations.	37
22. Major cycle crack growth in Ti-6Al-4V by cyclic cleavage and microvoid coalescence.	37
23. Minor cycle crack growth in Ti-6Al-4V by cyclic cleavage.	39
24. Major-minor cycle crack growth in Ti-6Al-4V by cyclic cleavage and block striations.	39
25. Comparison of macroscopic and microscopic FCG rates for Ti-6Al-4V.	40
26. Longitudinal section through a Ti-6Al-4V fracture surface showing cyclic cleavage of the primary α grains.	42
27. Longitudinal section through a Ti-6Al-4V fracture surface showing that block striations are unrelated to the underlying microstructure.	42
28. Transmission electron fractograph of a block striation plateau in Ti-6Al-4V.	43
29. Transmission electron fractograph showing parallel ripple markings between block striations in Ti-6Al-4V	43
30. Major cycle growth in Ti-5331S producing transgranular facets striation plateaux, microvoid coalescence and fretting oxidation-debris.	44
31. Division by tear ridges of a large striation	44

LIST OF ILLUSTRATIONS (CONTINUED)

	PAGE
plateau in Ti-5331S.	
32. Curvilinear striations superimposed on a cyclic cleavage facet in Ti-5331S.	45
33. Large brittle striations continuous with finer ductile striations in Ti-5331S.	45
34. Transmission electron fractograph of a striation plateau in Ti-5331S.	46
35. Brittle striations in Ti-5331S showing the development of tear ridges at block striations.	46
36. Dependence of fatigue threshold upon stress ratio predicted by the crack closure model.	50
37. Continuous dependence of fatigue threshold on stress ratio.	50
38. Variation in fatigue threshold value with stress ratio for titanium-based alloys.	51

LIST OF TABLES

TABLE	PAGE
1. Comparison of experimental and predicted values of ΔK_{onset} for Ti-6Al-4V.	8
2. Fatigue threshold values in Ti-5331S.	16
3. Comparison of methods for determining ΔK_{onset} .	23
4. ΔK_{onset} values for Ti-5331S.	23

SECTION 1

INTRODUCTION

The disintegration of an aeroengine disc is one of the few examples of a single component failure which can endanger an aircraft and its occupants. Another example is the loss of a fan blade. Currently these expensive components are retired from service on a time expired basis, the safe life being calculated from a low cycle fatigue (LCF) analysis. This procedure has undoubtedly achieved a high level of reliability and safety, but it also imposes a considerable financial burden. An inspection of 1000 retired discs is likely to show that only one contains a crack of engineering dimensions. The remainder have been prematurely retired. Their useful residual life may be realised only by applying a policy known either as on-condition lifing or retirement for cause(1).

Retirement for cause is a fracture mechanics based lifing policy which enables a greater proportion of the available life of critical rotating aeroengine components to be realised. The inspection period, or return to service interval, is related to that part of a component's fatigue life which can readily be described by fracture mechanics, namely, its crack propagation life. In the first instance this can be considered to be the number of flights, or LCF events, required to grow a crack from a size which is just below the limits of confident detection by non-destructive evaluation, to a larger critical size. Within this life span there must be fitted an appropriate number of economic inspection intervals.

All engine flight patterns involve take-off and landing, with various cruise conditions in between. Such a pattern can be represented simplistically by a trapezoidal waveform as shown in Figure 1a. The forces build up to a maximum during take-off, OA; remain essentially constant during cruise, AB; and return to zero when the aircraft lands and the engine is switched-off, BC. At a critical region in a disc, say at a blade attachment, the changes in centrifugal and thermal stresses, corresponding to the start-stop operation (called the major cycle), are the principal sources of damage responsible for low cycle fatigue life limitation(2). During the dwell period (cruise conditions), it is possible that some creep or stress relaxation might occur in the locally highly stressed region. Also, in reality, small amplitude vibrational stresses of high frequency (equal to some multiple of the blade passing frequency) will be superimposed on the major cycle, as indicated in Figure 1b. They are responsible for high cycle fatigue (HCF) damage.

The application of a policy of retirement for cause requires a knowledge of the fatigue crack growth (FCG) behaviour in disc and blade materials. Inevitably this will include an assessment of the effect on FCG of small amplitude, high frequency, stress cycles which are vibratory in origin(3-5). How these minor, HCF, stress cycles modify the FCG behaviour associated with the major LCF loading is the subject of this study.

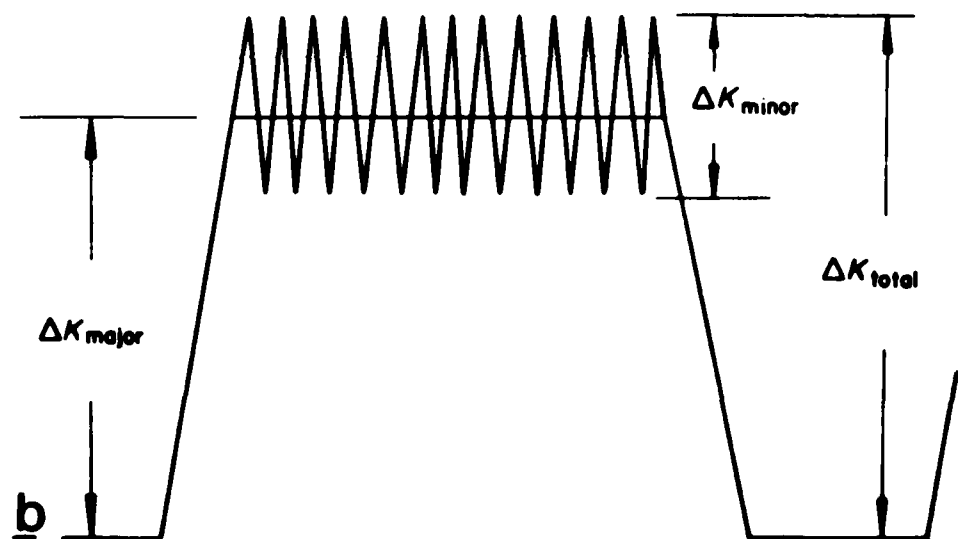
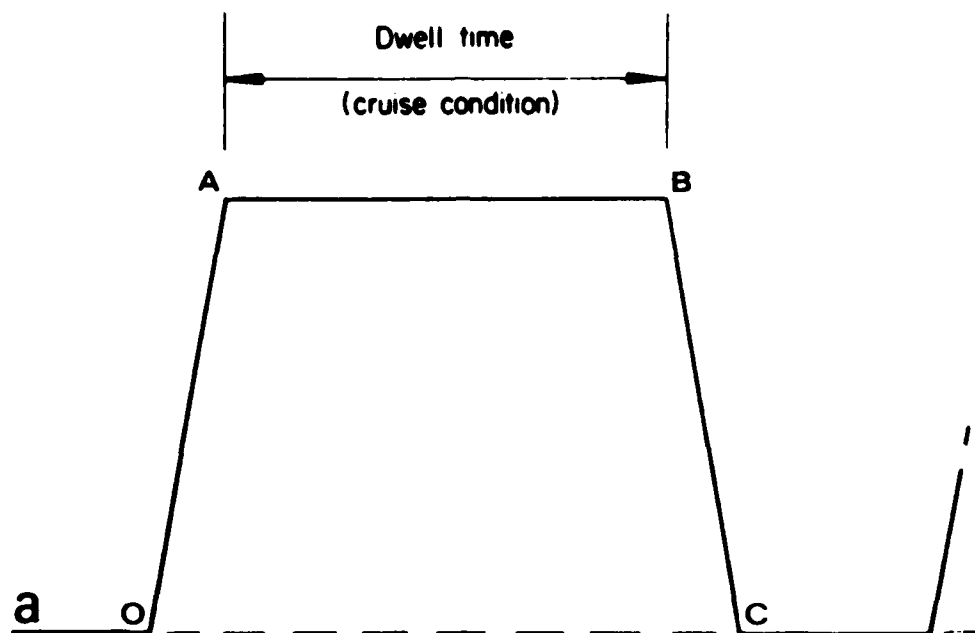


Figure 1 Load sequences: (a) major cycle only, (b) minor cycles superimposed on the dwell period of the major cycle.

SECTION 2

OBJECTIVES AND APPROACH

The work described in this report forms part of a continuing study(3-5) concerned with the propagation of fatigue cracks. The overall aim is that of measuring, and ultimately predicting, the effects of the conjoint action of major and minor stress cycles on the life of rotating aeroengine components whose design and operation is based upon the philosophy of retirement for cause.

A major-minor cycling test facility has been specifically developed which allows the application of combined low frequency major and high frequency minor cycles. The system consists of an electromagnetic vibrator mounted on a servohydraulic testing machine in line with the actuator. A vibration isolator transmits the major load from the actuator to the test specimen, whilst allowing the high frequency movement of the vibrator(6). The major and minor loading components may be applied independently and without interaction.

Compact tension (CT) test pieces having a width of 26 mm, thickness of 13 mm, and conforming to the ASTM(7) specified design have been cut from radial slices from a Ti-6Al-4V fan disc and a Ti-5331S high pressure compressor disc.

In the crack growth experiments, the major cycle experienced by the critical rotating aeroengine components is represented simplistically by a trapezoidal stress wave (Figure 1a) having the following characteristics:

Rise time:	1.0 s	Rest period:	1.2 s
Fall time:	1.0 s	Frequency:	0.1 Hz
Dwell period:	6.8 s	Stress ratio:	0.1

The crack extension rates produced by the repeated application of this major stress cycle are determined, having first precracked the CT specimens to give a normalised crack length of about 0.3.

A minor cycle is a high frequency sinusoidal stress wave of constant amplitude, and initially a frequency of 150 Hz has been adopted. Fatigue threshold levels and near-threshold FCG rates are obtained for a separate minor cycle loading following a conventional precracking and load shedding sequence. The minor cycle stress ratios employed are those associated with the minor cycles used in tests involving the conjoint action of major and minor cycles(4).

The combined major-minor cycle or loading block is generated by the synchronised addition of the major and minor cycles, generally restricting the minor cycles to the dwell period (Figure 1b). Allowing for the build-up and decay of the minor cycles, a frequency of 150 Hz and a dwell period of 6.8 s will give an effective 1000 minor cycles per major cycle dwell. By lengthening the dwell period, or by alter-

ing the minor cycle frequency, other cycle ratios (n) are obtained. Initially three levels of minor cycle loading, typical of some service conditions, have been adopted, namely, minor/major amplitude ratios (Q) of 0.12, 0.22 and 0.32.

Testing under the conjoint action of major and minor stress cycles generally requires a precracking and load shedding schedule. During the subsequent collection of FCG data, the levels of major and minor stress amplitude are maintained constant and as the test proceeds the associated levels of stress intensity range rise with the accelerating crack advance. Where possible, the approach adopted is to grow the crack from a low level of stress intensity range at which the minor cycles are inactive, and by virtue of the consequential rise in stress intensity range, establish both the condition at which the minor cycles become active and the resulting crack growth rates.

During every test, crack length is monitored using the direct current potential difference (DCPD) technique. The three-point secant method is used to obtain crack growth rates, with input data corresponding to equal increments in the observed DCPD voltage ratio.

SECTION 3

CRACK GROWTH IN Ti-6Al-4V

3.1 EFFECT OF AMPLITUDE RATIO AND CYCLE RATIO

Fatigue crack propagation experiments have been undertaken using 10,000 minor cycles superimposed on the dwell period of the major cycle, with minor to major amplitude ratios of 0.12, 0.22 and 0.32. The recorded growth rates, shown in Figure 2, are presented as a function K_{total} since this parameter accounts for the increase in stress intensity range resulting from the superimposition of the minors on the major cycle. Data for major cycle loading only ($Q = 0$) are included for comparison. Figure 2 shows that the effect of increased amplitude ratio is to give an enhanced FCG rate. Similarly, Figure 3 shows the enhancement in FCG rate associated with an increase in cycle ratio from $n = 1000$ to $n = 100,000$ for a constant and low value of amplitude ratio. Data for major cycle loading only ($n = 0$) are again included for comparison. In each figure, it is evident that enhanced FCG rates only occur above a transition level of ΔK_{total} , and that this transition is dependent upon the amplitude ratio but insensitive to variations in cycle ratio. This transition has been labelled ΔK_{onset} since it corresponds to the onset of minor cycle fatigue damage.

3.2 THE ONSET OF MINOR CYCLE ACTIVITY

It is apparent from the waveform of the combined major and minor stress cycles (Figure 1b) that:

$$\Delta K_{total} = \Delta K_{major} + \frac{1}{2} \Delta K_{minor} \quad \text{..... (1)}$$

Since the relationship between the minor and major stress waves is given by the amplitude ratio, then:

$$\Delta K_{total} = \{(2 + Q)/2Q\} \Delta K_{minor} \quad \text{..... (2)}$$

The parameter ΔK_{onset} is defined as the value of the total or overall stress intensity range associated with combined major and minor stress cycles at the point where the minor cycles become active. Assuming that the minor cycles become active when they reach their threshold value, this parameter may be calculated from the expression:

$$\Delta K_{onset} = \{(2 + Q)/2Q\} \Delta K_{th \text{ minor}} \quad \text{..... (3)}$$

where $\Delta K_{th \text{ minor}}$ is the fatigue threshold value for the minor cycles which typically possess a stress ratio in excess of 0.7.

The tests involving 10,000 minor cycles per major have been designed to give an experimental determination of ΔK_{onset} . Crack formation is achieved with a high frequency sinusoidal waveform. The subsequent precracking step down sequence employs a low frequency trapezoidal wave, with 10% reductions in loads, until the level of ΔK is below

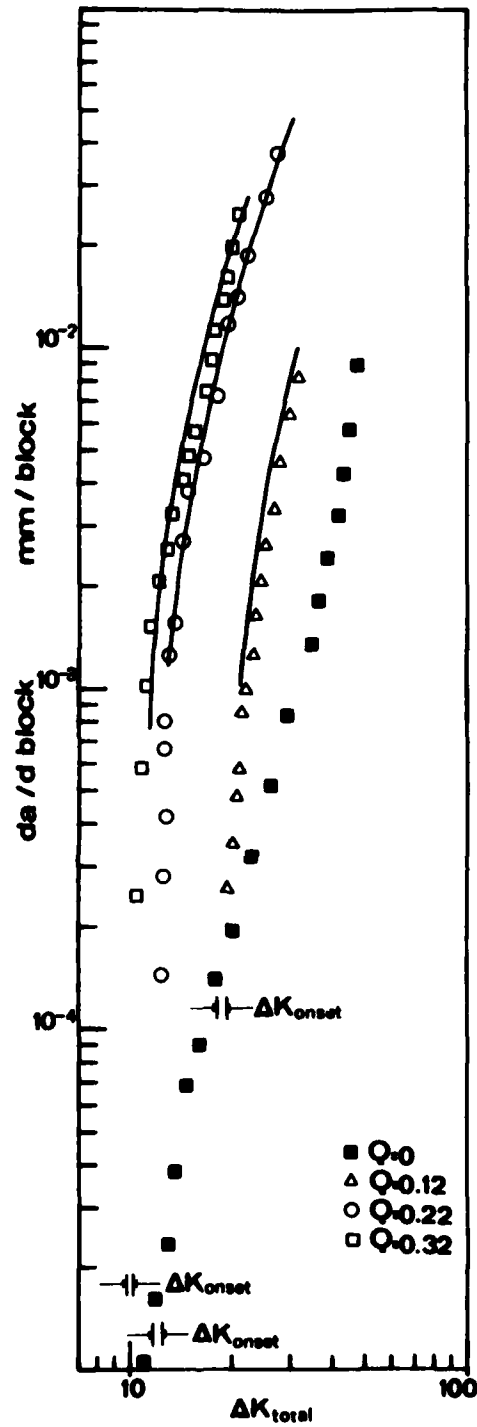


Figure 2 Effect of amplitude ratio (Q). Data for Ti-6Al-4V and a cycle ratio of 10 000. The lines indicate the linear summation predictions.

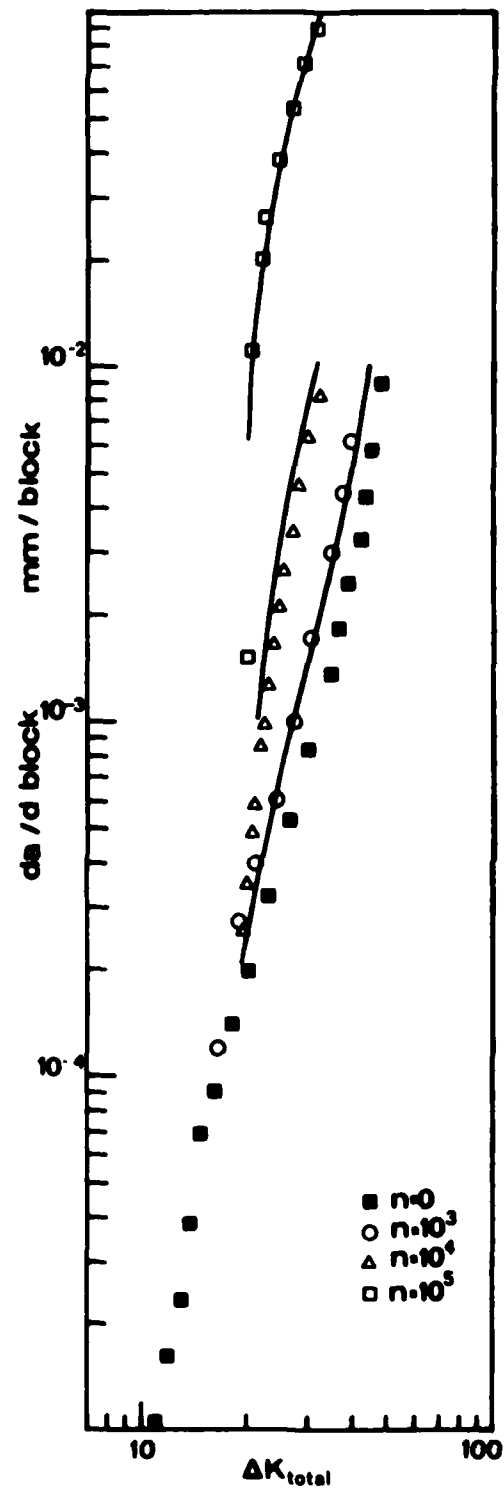


Figure 3 Effect of cycle ratio (n).
Data for Ti-6Al-4V and an amplitude ratio of 0.12.

the value of ΔK_{onset} predicted by a modified form of Equation 3.

$$\Delta K_{\text{onset}} = \{(2 + Q)/2Q\} \bar{\Delta K}_{\text{th}} \quad \text{..... (4)}$$

The parameter $\bar{\Delta K}_{\text{th}}$ is the mean value of threshold stress intensity range, at the stress ratio of the minor cycles, obtained from a simple linear regression analysis of threshold value versus stress ratio data. Having completed the precracking a combined major and minor loading is applied, and a prolonged period of testing, in excess of 8 h, is used to confirm the absence or existence of minor cycle activity.

During the 8 h period there are 400 major cycles and 4 million minor cycles, as compared to a value of 10 million cycles conventionally used in a threshold test. If the minor cycles are inactive then the number of major cycles at the prevailing level of ΔK_{total} is insufficient to produce any detectable crack growth. In this case the loading is increased by 5-10% and the process repeated. Once the fatigue damage due to the minor cycle activity is apparent, the crack is allowed to grow without interruption at the prevailing load level. Finally, ΔK_{onset} is taken to be the value of ΔK_{total} intermediate between the maximum value at which the minor cycles were considered to be inactive and the minimum value at which they clearly gave an enhanced growth rate (Figure 2).

The values of ΔK_{onset} obtained at amplitude ratios of 0.06, 0.12, 0.22 and 0.32, together with the values of ΔK_{onset} predicted from conventionally determined threshold data using Equation 4 are shown in Table 1. For the four amplitude ratios considered, the correlation is good.

Table 1. Comparison of experimental and predicted values of ΔK_{onset} for Ti-6Al-4V.

Amplitude Ratio	ΔK_{onset} (MPa $\sqrt{\text{m}}$)	
	Predicted	Experimental
0.06	33.3	33.4 \pm 1.1
0.12	18.5	18.8 \pm .7
0.12	18.5	18.5 \pm .5
0.22	11.9	12.1 \pm .3
0.22	11.9	12.2 \pm .3
0.32	9.4	10.0 \pm .2

3.3 PREDICTING FATIGUE CRACK GROWTH RATES

The prediction of FCG rates, by the linear summation of growth rates measured for the separate components of major and minor stress cycles(4), has been tested for several combinations of amplitude and cycle ratio. The analysis can be undertaken using the applied loading of one major cycle at ΔK_{major} and n minor cycles at ΔK_{minor} . Alternatively, if a rainflow counting technique is applied to the loading block, it is seen to be composed of one large cycle of ΔK_{total} interrupted by $n-1$ sub-cycles of ΔK_{minor} . This distinction is irrelevant for the conditions of $n = 10,000$ and $n = 100,000$ because the growth is predominantly due to the minor cycles once they are activated. However, the growth associated with 1000 minor cycles of low amplitude ($Q = 0.12$) is similar to that produced by the major cycle. In this case the method of assessing the major cycle damage is relevant, and a superior prediction is obtained using a rainflow scheme of cycle counting.

With regard to previously published work(4), the greatest discrepancy between predicted and experimentally measured growth rates occurred with a major-minor cycle loading of $Q = 0.22$ and $n = 1000$. In this case not only did the experimental data for the dual frequency loading show considerable scatter, but the prediction itself was based upon limited minor cycle growth rate data. This combination of major and minor loading has therefore been used in a re-assessment of the accuracy of linear summation predictions.

Figure 4 shows the accumulated results of both new and previous tests at the appropriate minor cycle stress ratio of 0.82. Also indicated is the visually fitted curve which is used to represent this data in an improved linear summation prediction. Crack growth results for three new tests at $Q = 0.22$ and $n = 1000$ are shown in Figure 5. This data falls within the wide scatter band of previous results, and it exhibits the same degree of reproducibility seen at the other amplitude ratios. Above all, the improved linear summation prediction now accurately describes the growth rates observed for this major-minor cycle loading condition (Figure 5).

Cycle ratios of 10,000 and 100,000 are achieved simply by extending the dwell period to accommodate the required number of minor cycles. Any modifications to the major cycle growth rate resulting from an extended dwell period is unimportant, because, even with a low amplitude ratio of 0.12, the number of minor cycles is such that the damage caused by the active minor cycle is dominant. Growth rate predictions are represented in Figures 2 and 3 by continuous lines. They show that the FCG rates for a wide range of amplitude ratio and cycle ratio are effectively predicted by the method of linear summation.

3.4 A LOW VIBRATIONAL AMPLITUDE

A reduction in vibrational amplitude has the significant effect of increasing the fatigue crack propagation life of a component subjected to combined high and low cycle fatigue. First, and most importantly in terms of an on-condition lifing policy, by delaying the onset of

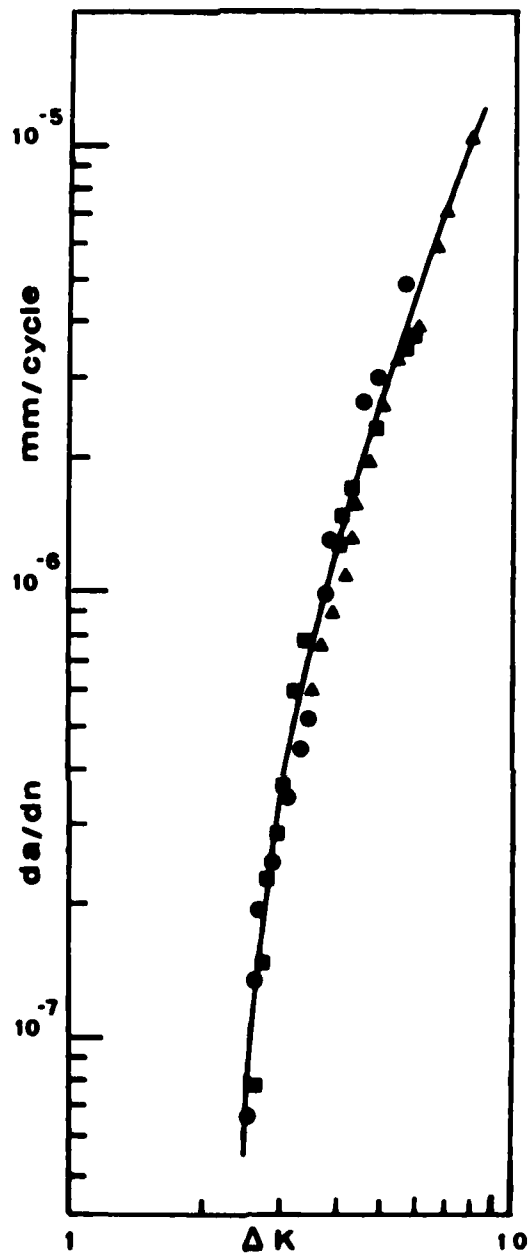


Figure 4 Near-threshold FCG data for Ti-6Al-4V at a stress ratio of 0.82. Data points for three tests. Line indicates the relationship used in calculating linear summation predictions.

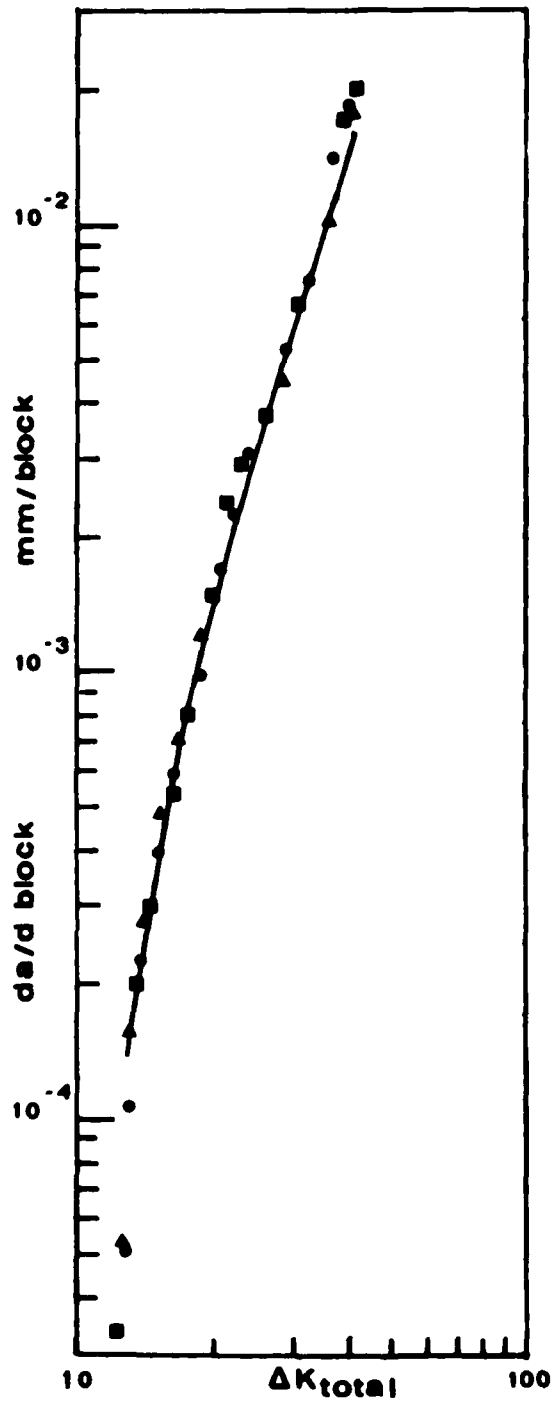


Figure 5 FCG rates in Ti-6Al-4V at an amplitude ratio of 0.22 and a cycle ratio of 1000. Data points for three tests. The line indicates the linear summation prediction.

high cycle fatigue damage, and second, by minimising the subsequent FCG rate. This behaviour has been clearly demonstrated for amplitude ratios of 0.32, 0.22 and 0.12; i.e., for minor cycle amplitudes which are 16%, 11% and 6% of the major cycle range. Some further exploratory tests have been used to confirm the benefits expected from low vibrational levels. In a test using an amplitude ratio of 0.06 (i.e., a minor cycle amplitude of 3% of the major cycle range) combined with a cycle ratio of 100,000, the onset of minor cycle activity was delayed until ΔK_{total} reached 33.4 ± 1.1 MPa/m. This was in agreement with the predicted value of 33.3 MPa. The prediction was again based on a threshold value obtained by fitting a linear relationship to the available ΔK_{th} versus R data(4). In a further test, with $Q = 0.06$ and at a reduced cycle ratio of 10,000, the minor cycle damage was insufficient to define ΔK_{onset} . The growth rates observed in this test were similar to, or even slightly below, those previously recorded for major cycle only loading.

3.5 THE EFFECT OF REST PERIODS

All previous tests have used a trapezoidal major cycle with a 1.2 s hold at the minimum load. This rest period is included within the major cycle as an acknowledgement of the delay occurring between successive engine missions. The effect on FCG rates of extending this rest period to 60 s (a fifty-fold increase) has been tested in an experiment employing an amplitude ratio of 0.32. With lower Q values the testing time becomes excessive. A serious breakdown of the electromagnetic vibrator occurred during prolonged testing at $Q = 0.22$, thereby limiting the crack growth data to a narrow range of ΔK . Figure 6 shows that the extension of the rest period gives a marginal reduction in the growth rates at the higher amplitude ratio.

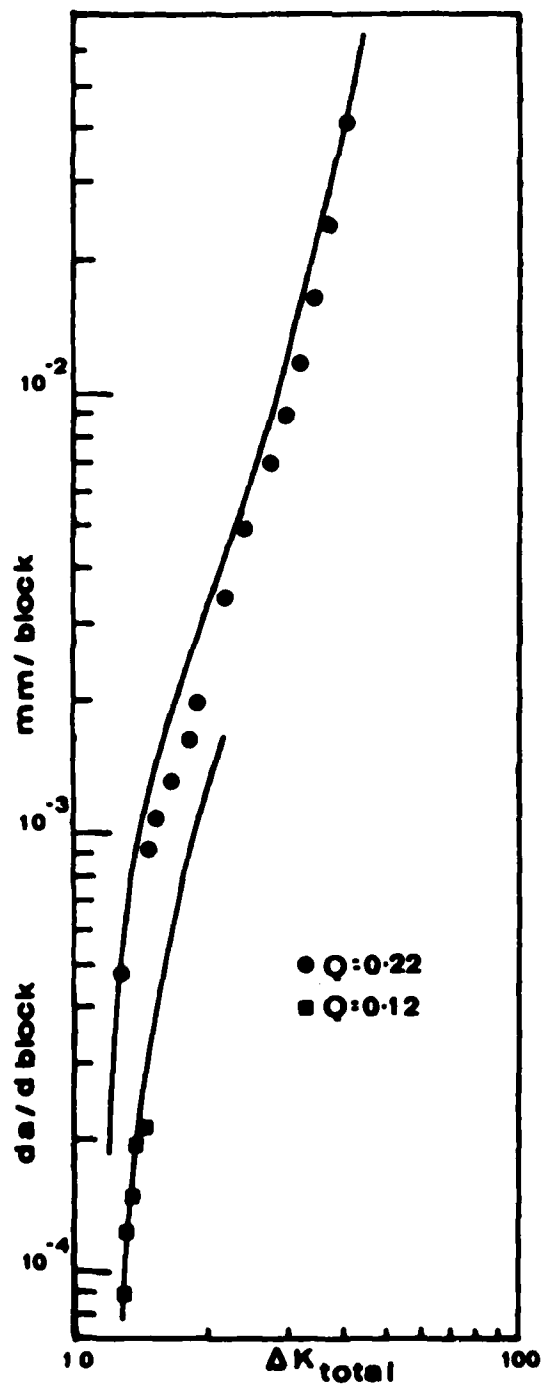


Figure 6 Effect of rest period. Data for Ti-6Al-4V at a cycle ratio of 1000. Data points are for a 60s rest period, the lines are for a 1.2s rest period.

SECTION 4

CRACK GROWTH IN Ti-5331S

4.1 INTRODUCTION

Creep resistant titanium alloys are essential to the design of light-weight aeroengines. The development of these alloys have been such that they have replaced discs and blades previously made of heavier materials(8), and further replacements are possible. They contrast strongly with Ti-6Al-4V for their microstructure is predominantly α and their grain size is large. By virtue of this microstructure, such alloys can show substantial load transfer across crack faces. This will influence the amount of crack closure, and hence both threshold values and fatigue crack growth (FCG) rates(9). Relative to Ti-6Al-4V data a greater scatter in FCG rates is to be expected. Given these significant differences, it is considered desirable that the key findings on major-minor cycling, obtained with Ti-6Al-4V specimens, are re-evaluated using a creep resistant titanium alloy.

The second material tested is Ti-5331S, the recently developed high temperature disc and blade material selected for future use in aero-engine construction. It is capable of continuous operation at 550°C, with low stress excursions to 600°C, this high temperature performance having been achieved in three steps. First, through the development of near- α microstructures. The amount of α phase is increased because of the greater creep resistance of this phase. Sufficient β stabiliser is added to retain a small amount of β , so ensuring that the alloy can still be heat treated and forged. The α phase is solution strengthened by the maximum possible addition of several α stabilisers, consistent with the complete avoidance of embrittlement associated with an ordered crystal lattice(10). Second, these alloys are used in the β heat treated form. As a consequence, the normal microstructure of primary α and transformed β is replaced by a fully transformed β structure characterised by a basketweave α morphology. Third, the composition has been progressively optimised. Thus Ti-5331S, consisting of Ti-5.5Al-3.5Sn-3Zr-1Nb-0.25Mo-0.3Si has been developed from the currently used near- α alloy, Ti-65S, which contains Ti-6Al-5Zr0.5Mo-0.3Si. Reaction rates have been further reduced by the addition of heavy tin, whilst the addition of niobium gives a greater oxidation resistance and so mitigates the effects of α case.

4.2 LOW CYCLE FATIGUE CRACK GROWTH

Major cycle fatigue crack growth rates corresponding to stress intensity ranges above 24 MPa \sqrt{m} have been measured for Ti-5331S, and found to be less than those observed for Ti-6Al-4V (Figure 7). Room temperature FCG rates for Ti-5331S forged disc materials have also been reported by Duncan et al(11) who cut specimens from two discs, and subjected them to a trapezoidal stress wave of 15 cpm and 1.6 s dwell on maximum load. Their accumulated crack growth data are represented by a wide scatter band. When the dwell on maximum load was extended to 5 mins the FCG rates tended to fall in the upper part of the 15-cpm

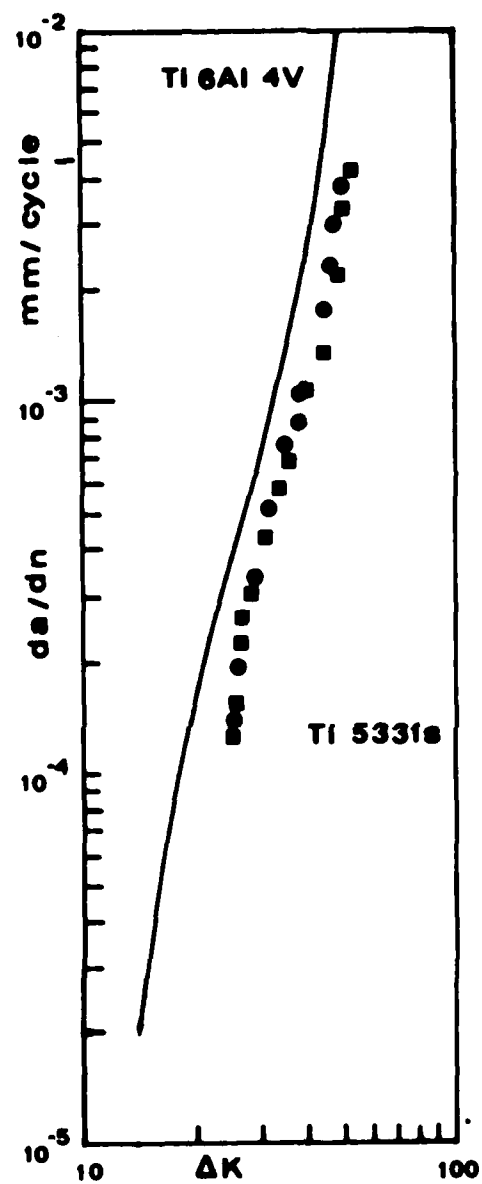


Figure 7 Major cycle FCG rates for Ti-6Al-4V and Ti-5331S at a stress ratio of 0.1.

scatter band, and they consequently represented all the results by a single composite scatter band. Figure 8 shows that the major cycle FCG rates determined in this project using a 6.8 s dwell on maximum load also fall close to the upper bound of the 15 cpm scatter band reported by Duncan et al(11).

4.3 HIGH CYCLE FATIGUE CRACK GROWTH

Fatigue threshold values (ΔK_{th}) and near-threshold FCG rates resulting from the application of high frequency minor cycles have also been measured in Ti-5331S. For the test conditions of $R_{major} = 0.1$, and minor to major amplitude ratios of 0.22 and 0.12, the minor cycle stress ratios are 0.82 and 0.90.

Table 2 shows the fatigue threshold values obtained at high stress ratios and a frequency of 150 Hz. The recorded values are marginally greater than those measured in Ti-6Al-4V(4).

Table 2. Fatigue threshold values for Ti-5331S.

Stress Ratio R_{minor}	Threshold Value ΔK_{th} (MPa \sqrt{m})
0.80	2.50
0.82	2.45
0.90	2.30
0.90	2.32

Having confirmed the existence of a fatigue threshold by repeatedly raising and lowering ΔK , the applied loads are again raised by the minimum amount necessary to restore crack growth. The FCG rates thus obtained for the near-threshold regime at stress ratios of 0.82 and 0.90 are presented in Figures 9 and 10. It is this data which is used in linear summation predictions for FCG rates under combined major-minor cycle loading.

4.4 CRACK GROWTH UNDER COMBINED LOW AND HIGH CYCLE FATIGUE

If ΔK_{onset} is to be determined from a single test in which the value of ΔK continually rises, then there must be a clear change in the FCG rate at the level where the minor cycles become active. If initially the minor cycles are inactive, the growth rate will be in response to the applied ΔK_{total} associated with the combined major and minor stress cycles. A large number of minor cycles, and hence a long dwell period, will only result in prolonged testing times. At the same time, a low level of amplitude ratio is required to ensure that the minor cycles are triggered at a high level of ΔK_{total} , thus allowing

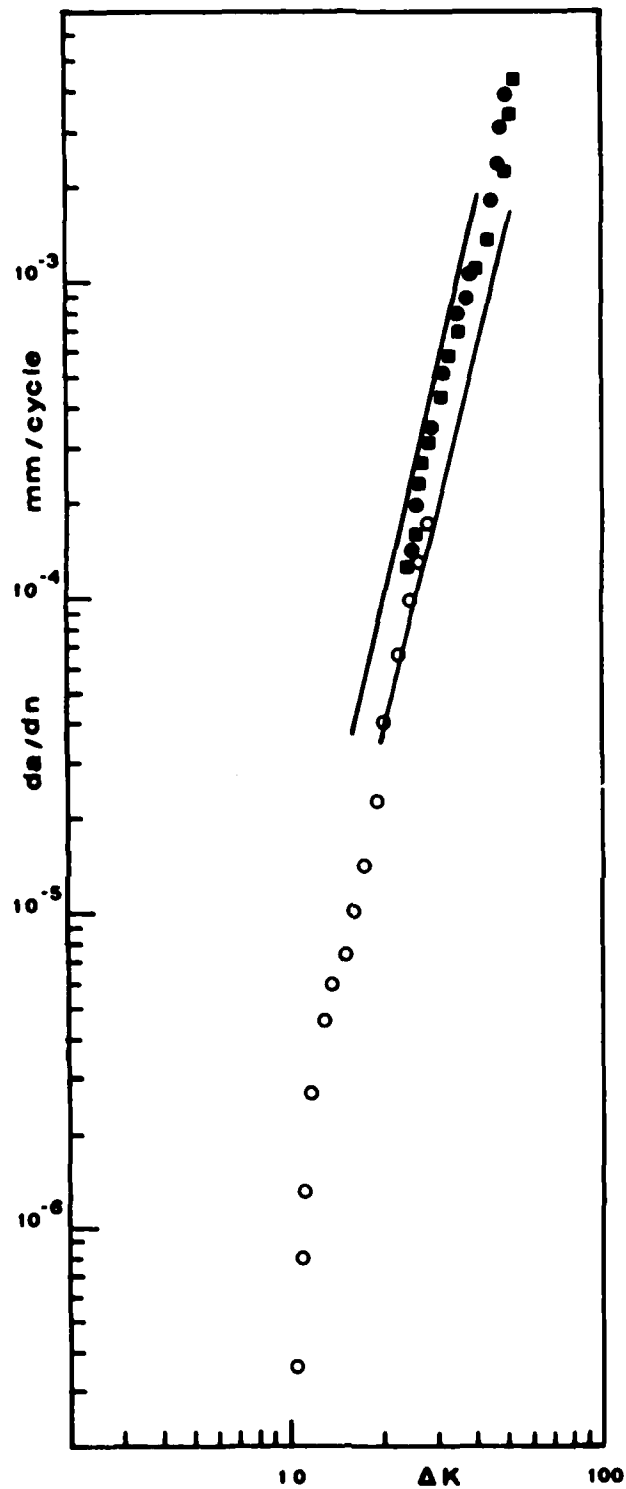


Figure 8 Comparison of major cycle growth rates for Ti-5331S. Closed symbols indicate 0.1-Hz data, open symbol indicates 150 Hz data. Lines show 15-cpm scatter band from reference 11.

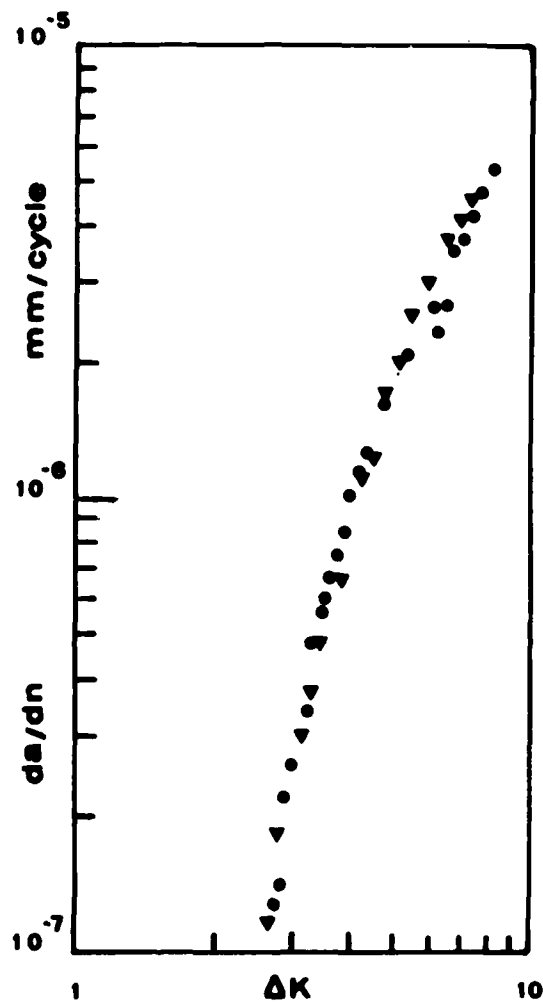


Figure 9 Near threshold FCG data for Ti-5331S at a stress ratio of 0.80 - 0.82. Data points for two tests.

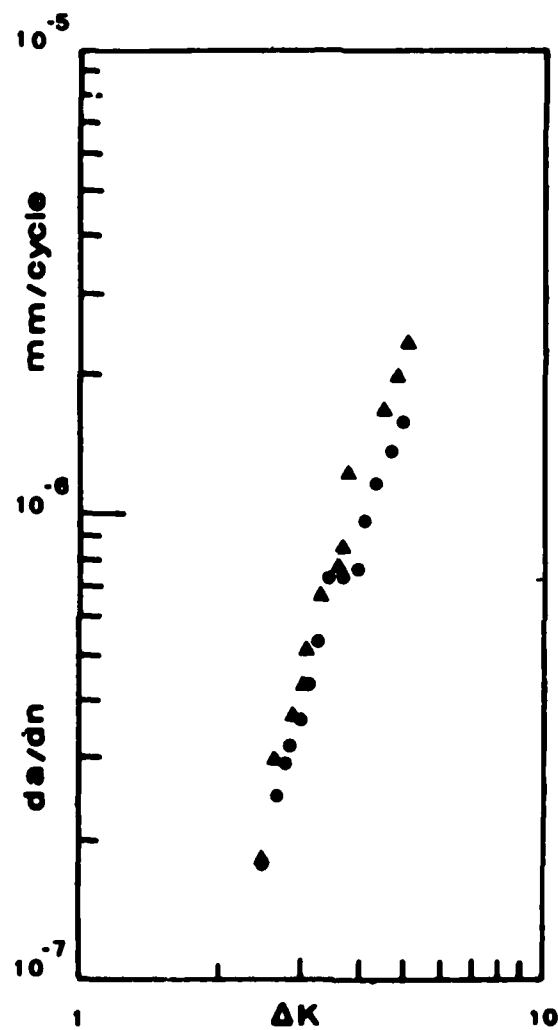


Figure 10 Near-threshold FCG data for Ti-5331S at a stress ratio of 0.90. Data points for two tests.

the collection of some growth data below ΔK_{onset} . However, to achieve a marked change in slope at ΔK_{onset} , and hence define it clearly, a large number of minor cycles having a high amplitude ratio is required in order to generate extensive minor cycle damage. Clearly such requirements are difficult to reconcile.

The development of a crack using a loading with a low stress ratio, followed by the testing of that crack under a combined major-minor cycle waveform at progressively higher stress intensities until the minors become active, is a reasonable approximation to the engineering situation which is being modelled. However this test procedure has been criticised on two counts. First, prolonged testing below ΔK_{onset} may influence the result. Hicks(12) has indicated that ΔK level may be raised by prolonged cycling below ΔK_{th} , at least for stress ratios where crack closure is present. Second, there is no confirmation of a ΔK_{onset} value arising from repeated raising and lowering of the applied loads, as is conventionally applied in threshold testing.

In view of these criticisms, and because of an experimental result which gave support to these ideas, an additional procedure for determining ΔK_{onset} has been used with Ti-5331S. It may be considered as a threshold test in which combined major and minor cycles are used throughout. Crack formation and load shedding are first accomplished using major-minor cycle waveforms having the chosen amplitude and cycle ratios. With 10,000 minor cycles per major cycle and $Q > 0.12$, a loading can eventually be found in which the combination of 10⁷ minor cycles and 1000 major cycles gives either no detectable growth, or growth which can be ascribed to the major cycle damage. The loadings are then increased by 5-10%, the minor cycle activity confirmed, and the crack then allowed to grow continuously without interruption at the prevailing loads. In this study these two methods for the experimental determination of ΔK_{onset} are defined as methods A and B, their procedural stages being summarised in Table 3.

Compact tension specimens of Ti-5331S have been used in the determination of ΔK_{onset} and the subsequent FCG rates for amplitude ratios of 0.12 and 0.22. Both test methods A and B have been employed. The accumulated FCG results are presented in Figures 11 and 12. The continuous lines included in these figures represent the growth rates predicted on the basis of the linear summation of major and minor cycle damage. Table 4 compares the experimental and predicted value of ΔK_{onset} for Ti-5331S.

It is clear from these results that the use of the threshold value for the minor cycles does not lead to an exact prediction of the onset of minor cycle growth under combined major and minor stress cycles. In all cases the experimental and predicted values are similar, but it would appear that the onset of minor cycle activity is to some degree retarded. Thus, the threshold-based predictions represent a conservative, or safe, estimate of the useful life of a Ti-5331S aeroengine component subjected to major-minor cycle loadings.

Much of the test data is so close to the linear summation predictions

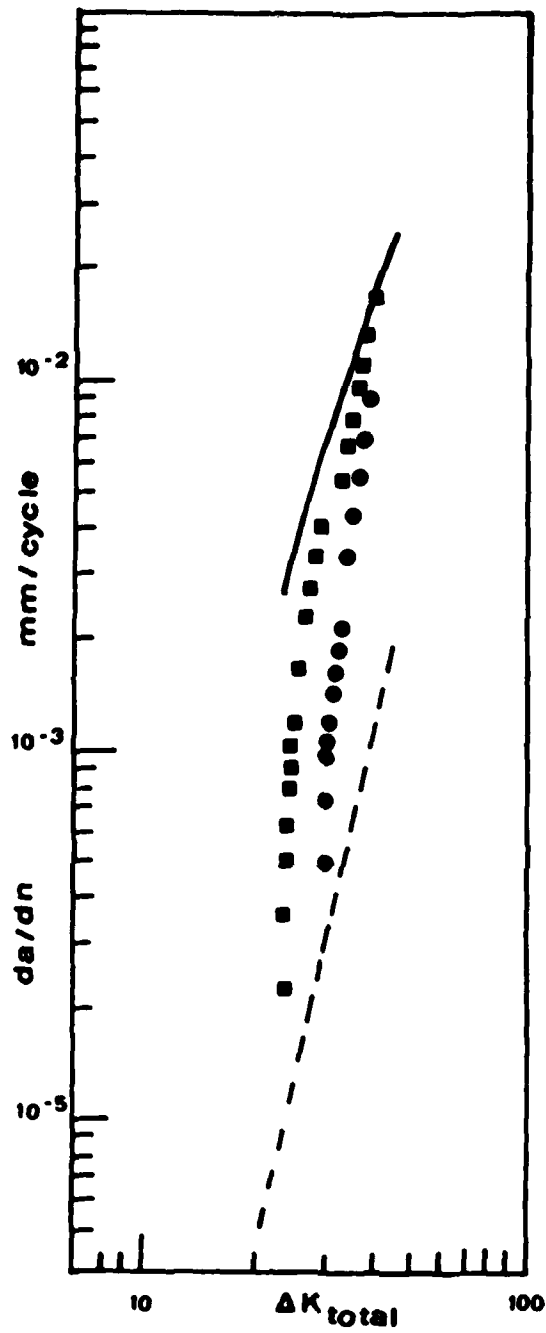


Figure 11 FCG rates in Ti-5331S at an amplitude ratio of 0.12 and a cycle ratio of 10,000. Key: ● = test method A, ■ = test method B, full line = linear summation prediction, chain line = major cycle data.

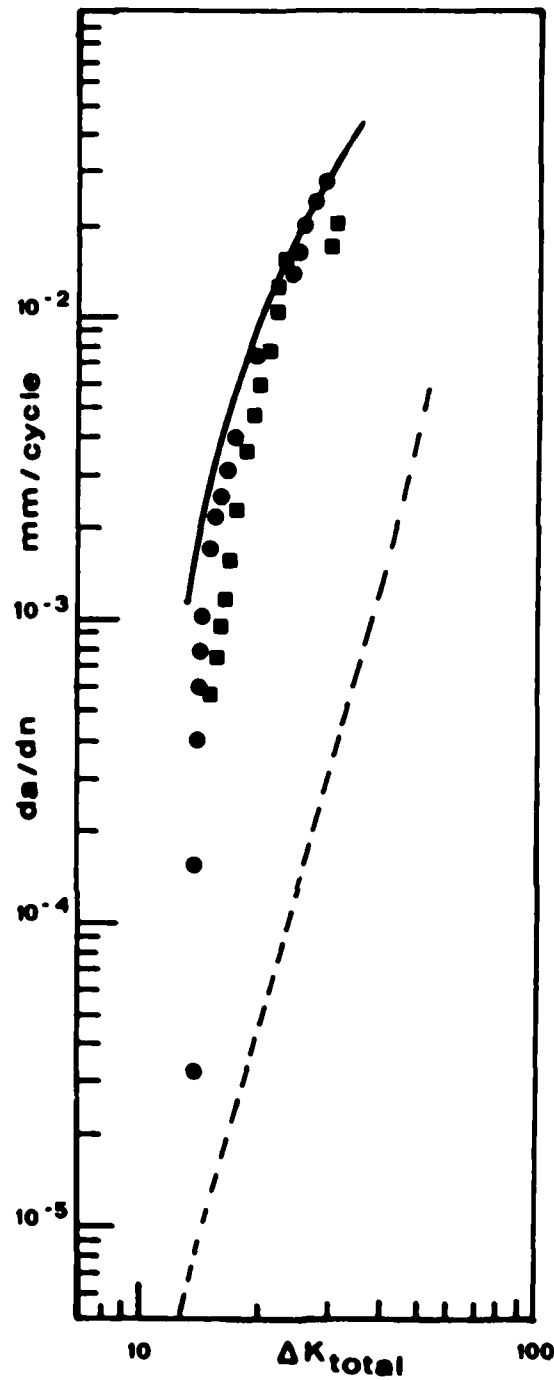


Figure 12 FCG rates in Ti-5331S at an amplitude ratio of 0.22 and a cycle ratio of 10,000.
Key: ● = test method A, ■ = test method B, full line = linear summation prediction, chain line = major cycle only data.

Table 3. Comparison of methods for determining ΔK_{onset}

Stage	Method A	Method B
Crack formation and load shedding sequence.	Pre-crack and load shed using a 150 Hz sine wave, $R = 0.1$. Essentially major cycle growth.	Pre-crack and load shed using a major-minor loading block, at $n = 10\,000$ and chosen Q value. Predominantly closure free minor cycle growth.
ΔK_{onset} determination.	Apply required major-minor loading block. Step-up loads periodically from below ΔK_{onset} until enhanced FCG rate is detected.	Conditionally step-down major-minor loading block until no growth or major only growth is observed. Step-up loads by 5-10% to confirm minor cycle activity.
Measurement of subsequent FCG rates.	Grow the crack at the prevailing loads.	Grow the crack at the prevailing loads.

Table 4. ΔK_{onset} values for Ti-5331S

Amplitude Ratio	Method	ΔK_{onset}	
		Predicted MPa/m	Experimental MPa/m
0.12	A	20.4	27.5 ± 2.4
0.12	B	20.4	22.6 ± 0.8
0.22	A	12.4	13.4 ± 0.7
0.22	B	12.4	13.2 ± 0.5

that it can reasonably be considered to be represented by it. The greatest discrepancy between predicted and experimental values occurs with an amplitude ratio of 0.12 when combined with test scheme A. During this test the loads were periodically raised until the value of ΔK_{total} exceeded the predicted value of ΔK_{onset} by 20%, with no clear indication of minor cycle growth. This test sequence was repeated at three different crack lengths with similar results. Eventually the loads were increased substantially and minor cycle growth was then quite evident. In due course the fracture surface of this specimen was seen to be unusually blackened over that region of the fracture surface where the attempts to find ΔK_{onset} lead to prolonged testing. This darkened fracture surface is probably the result of a build-up of oxide occasioned by repeated major cycle crack closure. It is estimated that the crack surfaces were closed more than 300,000 times prior to the active minor cycle crack growth.

The darkened fracture surface was eliminated by the use of test sequence B. In this case, precracking is largely achieved by fully open minor cycle crack growth, and the crack would now have closed fewer than 5000 times prior to the determination of ΔK_{onset} . The results of this test also show a closer agreement with all the linear summation predictions for this amplitude ratio. This response was not confirmed by the results for $Q = 0.22$. In this case a better correlation with the linear summation predictions was obtained with test sequence A, though neither sequence produced a darkened fracture surface.

SECTION 5

CRACK CLOSURE

Elber(13,14) was the first to observe that load transfer could occur across the fracture faces during the lower part of the fatigue cycle. The phenomenon, known as crack closure, has since been studied extensively. According to Elber crack closure was caused by the layer of residual plastic deformation left in the wake of the advancing crack front. More recent work has shown that mismatch of coarse fracture faces, as occurs in large grained titanium alloys, can give rise to high levels of crack closure(15-17). The concept of load transfer across closed crack surfaces has provided an explanation, at least in part, for the occurrence of threshold, stress ratio, and overload effects during fatigue crack propagation.

At the commencement of the test programme two assumptions regarding crack closure were made:-

1. That the minor cycles will be closure free by virtue of their high stress ratio ($R = 0.7$), but closure will occur within the major cycle ($R = 0.1$).
2. The closure load developed within the major cycle will be little affected by the addition of small amplitude minor cycles at the maximum dwell load.

Experimental evidence in support of these ideas will be presented in this section.

Closure plots are obtained by comparing the output from the load cell with that from a strain gauge located centrally on the back face of the CT specimen. Traces of load versus back face strain (BFS) are taken at increments in the DCPD voltage ratio of 0.05 (corresponding to crack length increments of approximately 0.6 mm). The closure plot is recorded on an X-Y plotter both on loading and unloading. In order to accommodate the slow response of the plotter it is necessary to make a temporary reduction in the rise and fall times and in practice, 11 seconds is used. Clearly the plotter cannot follow the high frequency minor cycles and the load range recorded is that of the major cycle.

Figure 13 shows a sequence of plots of load versus BFS obtained during crack growth tests in Ti-5331S at an amplitude ratio of 0.22. For each plot the crack opening load (P_{op}) is indicated, whilst the load range ($P_{max} - P_{min}$) is that of the applied major cycle. The closure load declines as the test proceeds, and as a consequence there is a progressive increase in the crack opening ratio (U), this being defined as:

$$U = (P_{max} - P_{op}) / (P_{max} - P_{min}) \quad \dots (5)$$

These trends are evident in all the tests examined despite the scatter in results for the specimens tested at the same nominal loading conditions.

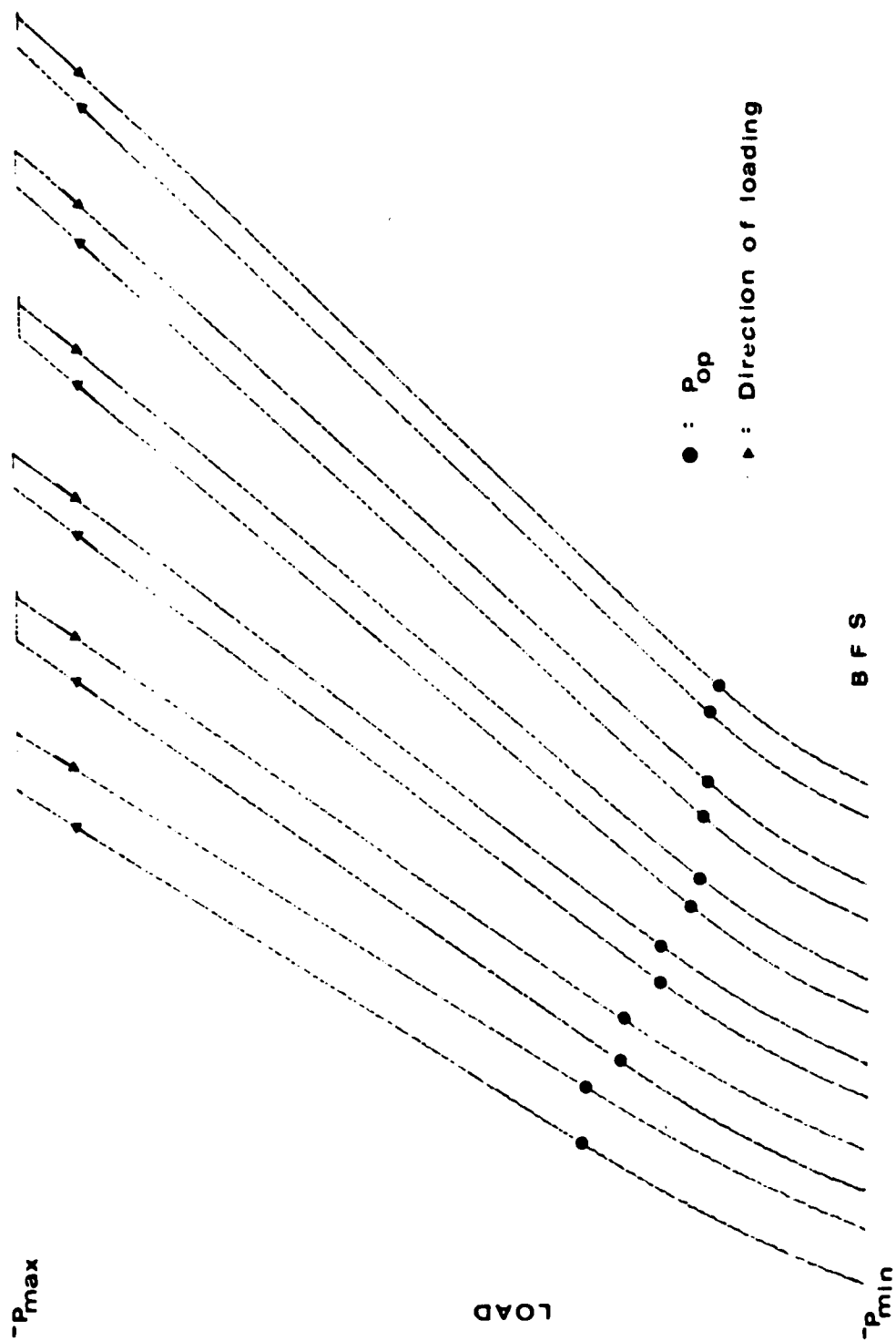


Figure 13 Sequence of load versus BFS traces at progressively greater crack lengths.

The decline in closure loads in association with an increase in crack length suggests that crack opening may correspond to the attainment of a fixed level of stress intensity(18). Figures 14 and 15 show that in CT specimens of Ti-5331S the opening of the crack does occur at a level of stress intensity (K_{op}) which is virtually constant. The results of repeated tests involving only major cycles, and combined major-minor cycle loadings, are illustrated. In each case the experimental points, which represent a bulk measurement of K_{op} , show a systematic variation about the indicated mean value. However, the superposition of minor cycles on the dwell period of the major cycle seems to have negligible effect upon either the constancy or level of K_{op} .

It is interesting to note that the crack opening behaviour of Ti-6Al-4V displays some characteristic differences. As expected, the levels of K_{op} observed are lower. However, each test exhibits a rise in K_{op} which is linearly related to ΔK (Figures 16 and 17). What is more, neither the magnitude nor the number of superimposed minor cycles alters this pattern of behaviour.

Crack opening ratios have been measured for trapezoidal loadings, using BFS gauges affixed to CT specimens of Ti-6Al-4V and Ti-5331S. On the assumption that a crack is able to grow only when its tip is open, it is reasonable to relate FCG rates to the effective range of stress intensity (ΔK_{eff}), this parameter being related to the applied stress intensity range by the expression:

$$\Delta K_{eff} = U \cdot \Delta K \quad \text{..... (6)}$$

The major cycle growth rates in Ti-6Al-4V and Ti-5331S coincide if plotted against ΔK_{eff} (Figure 18). The same behaviour has been reported by Halliday and Beevers(9) who compared growth rates in Ti-6Al-4V and the near- α alloy Ti-65S. Both sets of data suggest a slight divergence in growth rates at the highest level of ΔK_{eff} . These correlations emphasise the role of crack closure in influencing FCG rates in titanium-based aeroengine alloys.

Figure 19 shows the system used to monitor the occurrence or absence of crack closure during the application of the high-frequency minor cycle loading. The BFS gauge signal is again compared with the load cell output and after suitable amplification and adjustment the signals are displayed on a storage oscilloscope in the form of a load versus BFS plot (Figure 19a).

As an alternative, a compensated BFS signal has been used in a manner similar to that described by Kikukawa et al(19). The amplitude of the load signal is adjusted until it simulates the BFS output associated with an open crack, and at this stage the actual BFS signal is subtracted from the simulated signal. As a consequence, an oscilloscope trace of load versus compensated BFS indicates the existence of a fully open crack by a vertical line (Figure 19b). When the signal to noise ratio allows extensive amplification of the compensated BFS signal, this technique will produce a more accurate measure of the crack opening load.

Figure 20 shows the oscilloscope traces obtained by the two techniques

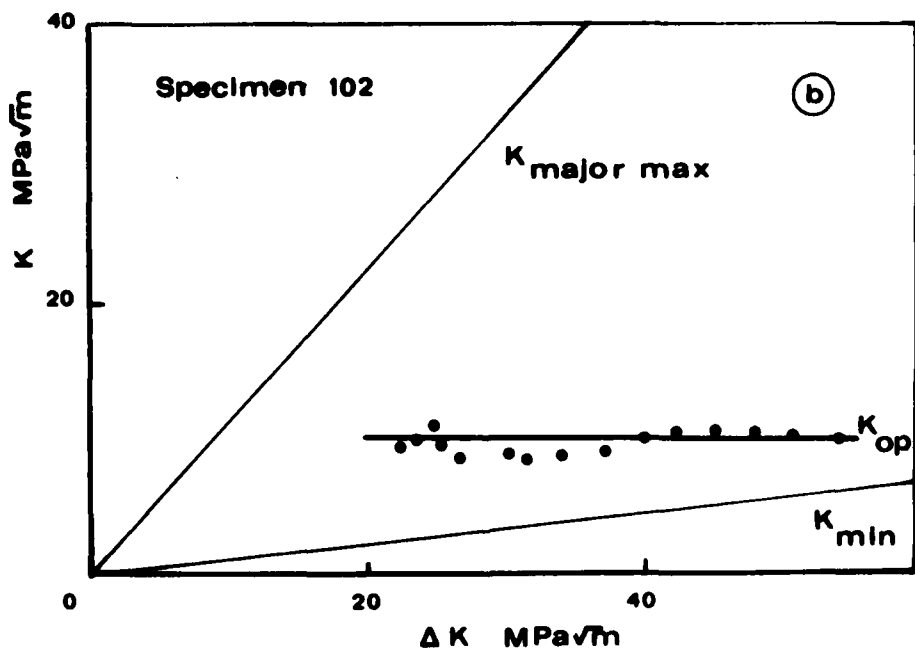
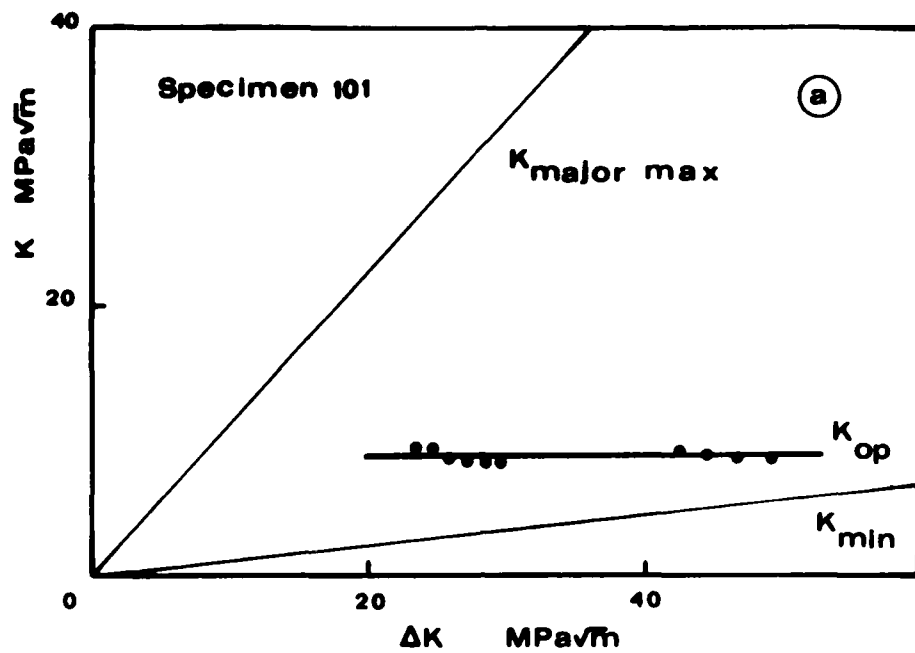


Figure 14 Crack closure behaviour in Ti-5331S for major cycle loading, duplicate tests.

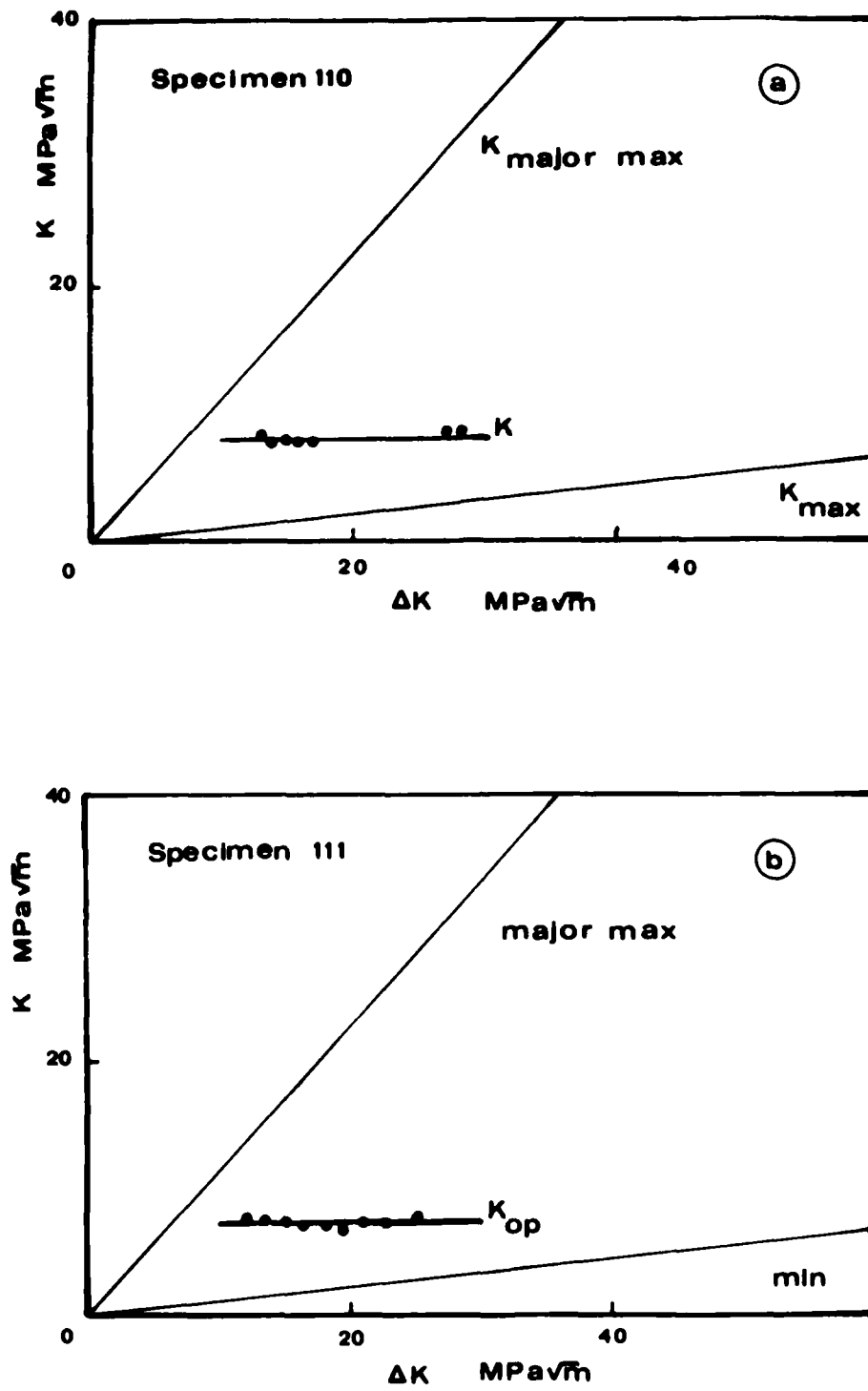


Figure 15 Crack closure behaviour in Ti-5331S for $Q = 0.22$ and $n = 10\,000$, duplicate tests.

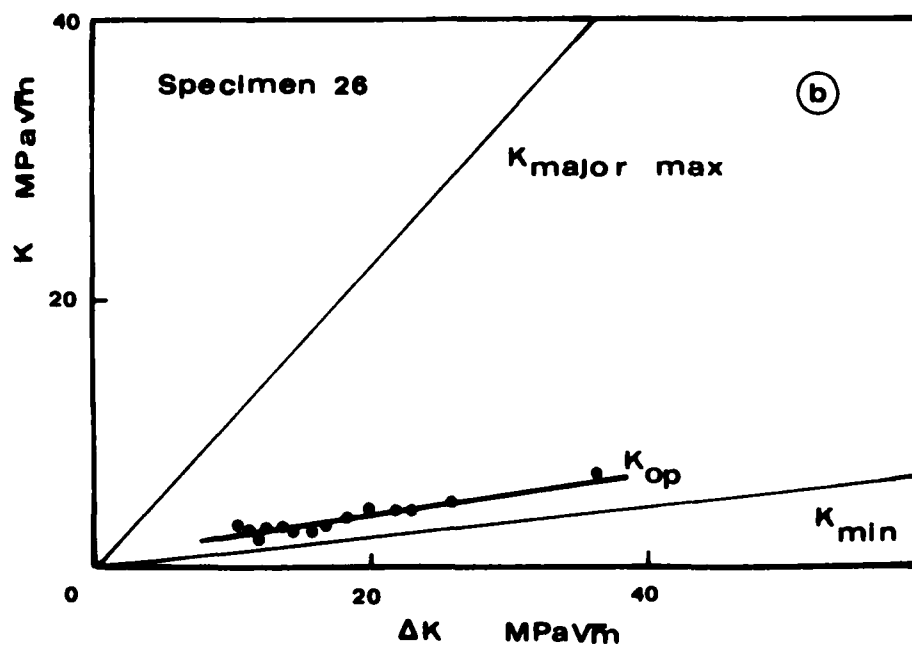
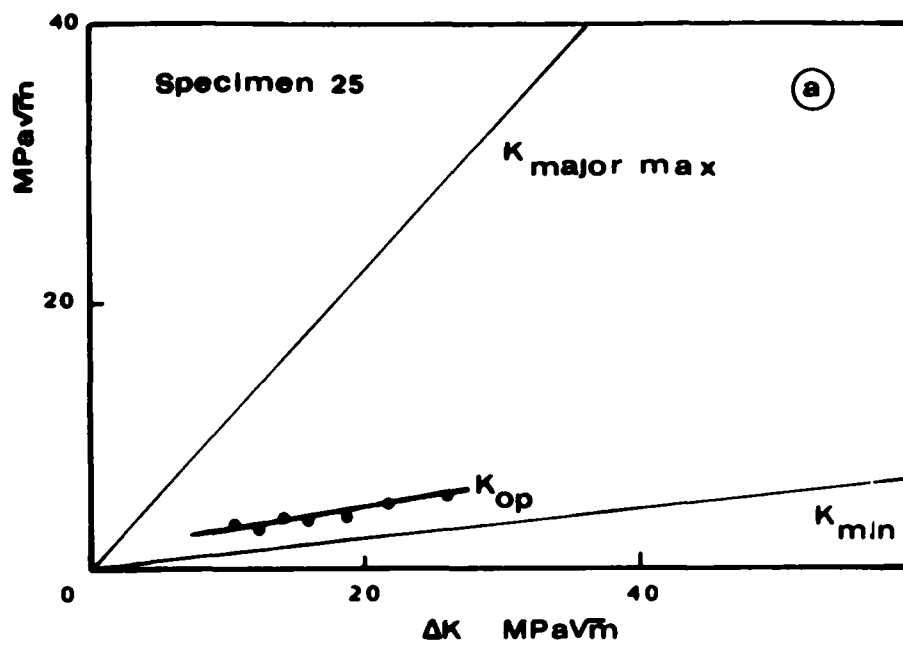


Figure 16 Crack closure behaviour in Ti-6Al-4V. (a) $Q = 0.33$ and $n = 1000$, (b) $Q = 0.32$ and $n = 1000$.

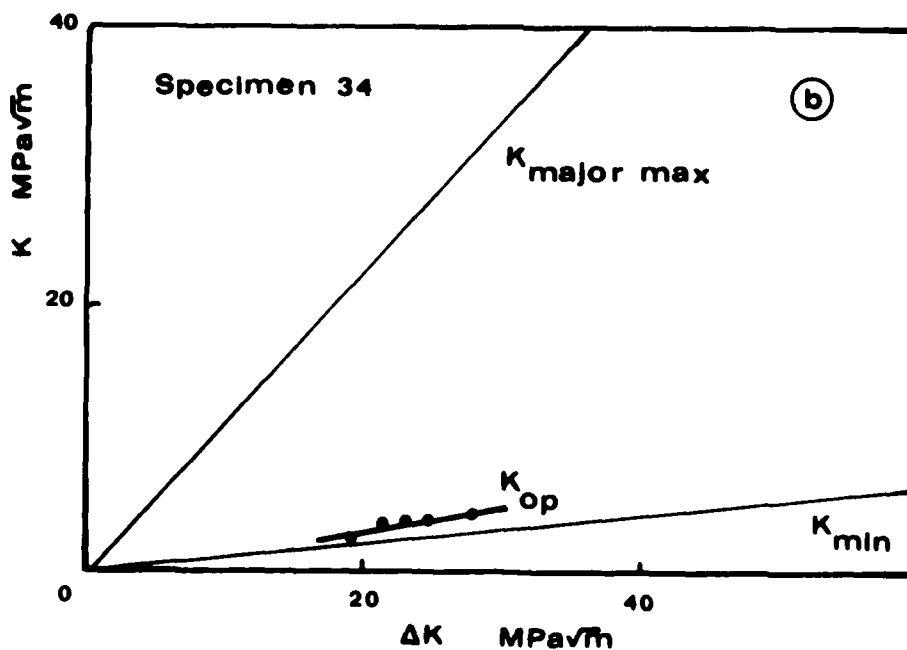
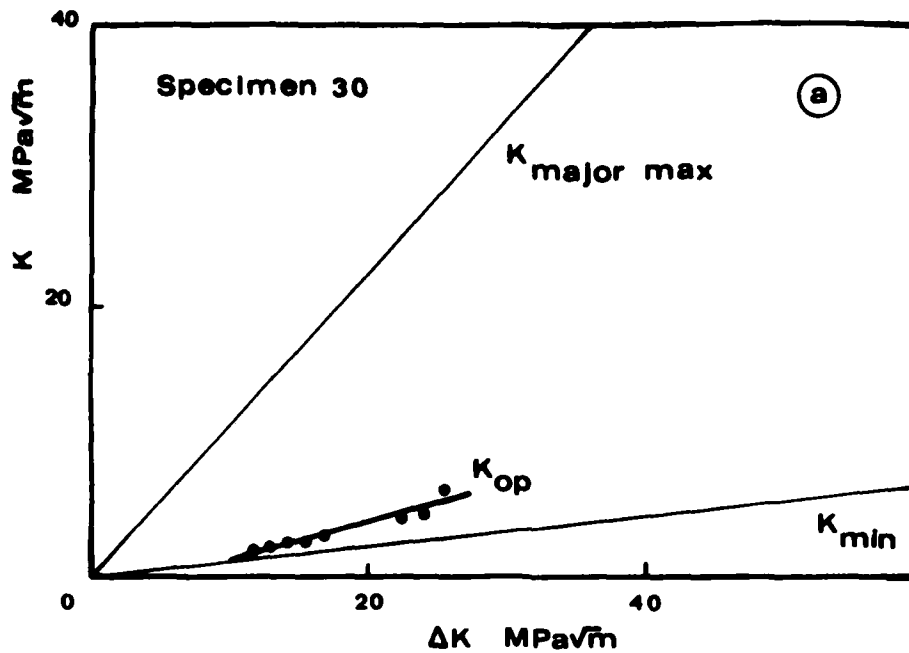


Figure 17 Crack closure behaviour in Ti-6Al-4V. (a) $Q = 0.22$ and $n = 10\,000$, (b) $Q = 0.12$ and $n = 100\,000$.

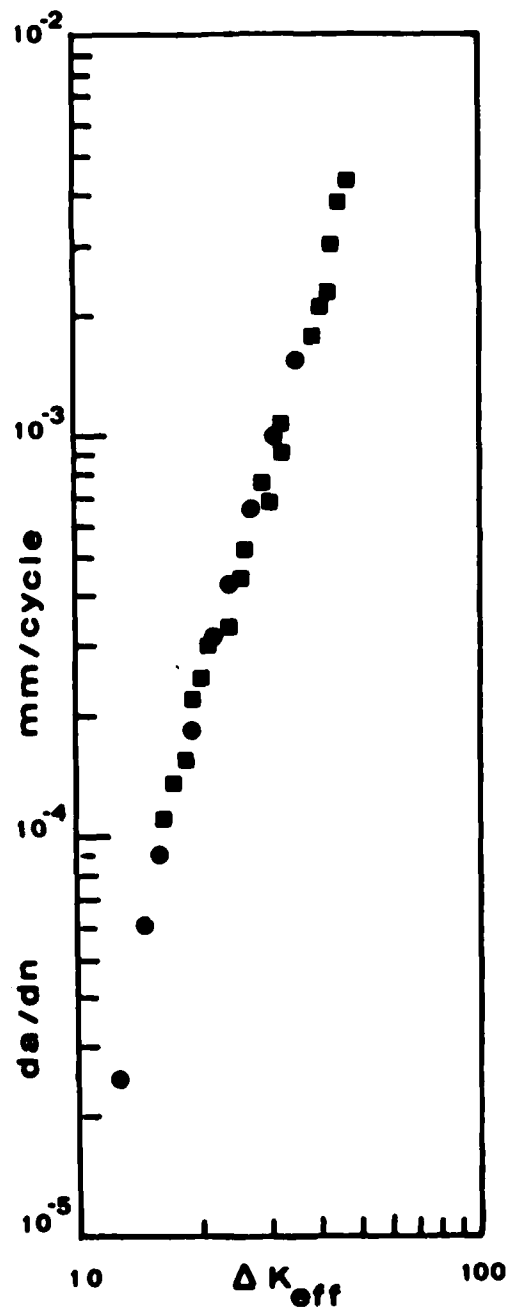


Figure 18 Correlation of FCG rates with ΔK_{eff} for two titanium alloys
 Key: ● = Ti-6Al-4V, ■ = Ti-5331S

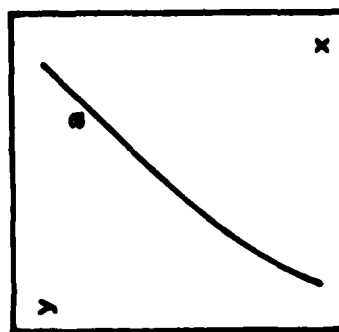
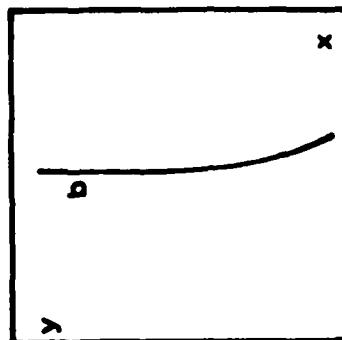
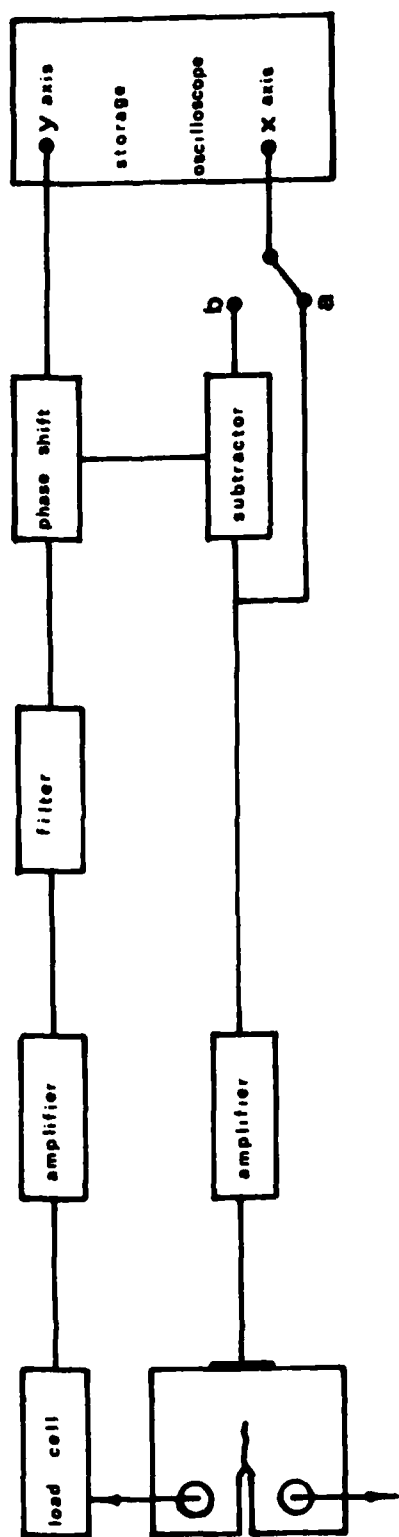
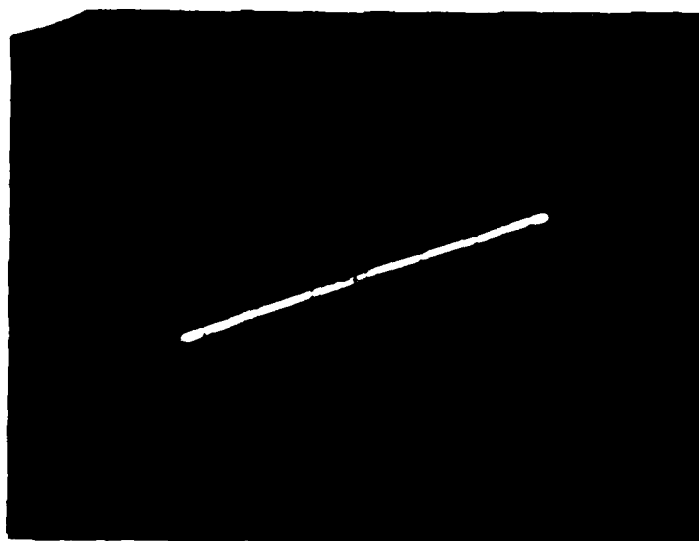
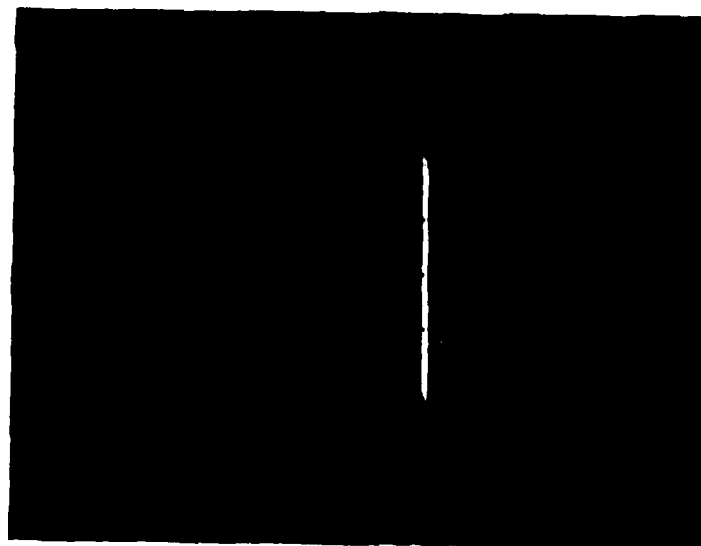


Figure 19 Schematic of dynamic closure monitoring system: (a) load versus BFS trace, (b) load versus compensated BFS trace.



a



b

Figure 20 Absence of crack closure in high frequency minor cycles.
(a) load versus BFS trace, (b) load versus compensated
BFS trace.

during a major-minor cycling test at an amplitude ratio of 0.12 and a minor cycle stress ratio of 0.90. As expected there is no evidence of crack closure associated with these minor cycles.

SECTION 6

FRACTOGRAPHIC STUDIES

6.1 INTRODUCTION

A more complete understanding of FCG behaviour can be achieved by combining the acquisition of growth rate data with a fractographic study of the test specimens. The growth rates measured at various ranges of stress intensity can then be related to the prevailing mechanism of crack advance. Consequently, the fracture surfaces of all crack propagation specimens tested in the current programme have been examined using a scanning electron microscope. In addition, the appearance of striated FCG has been investigated further using two-stage fracture surface replication in conjunction with a transmission electron microscope.

6.2 FATIGUE CRACKING PROCESSES IN Ti-6Al-4V

Crack growth rates have been obtained for a low frequency trapezoidal major cycle, at a stress ratio of 0.1, over the range $\Delta K = 13-50$ MPa/m. Cyclic cleavage facets (Figure 21) are observed at all levels of ΔK tested, being predominant below 16 MPa/m. Above this level, fatigue striations of classical form are observed. Using a working magnification of 1000 to 5000 times, the striations are initially revealed by the presence of periodic secondary cracks which develop from the troughs of some striations(20). At higher levels of ΔK the striations are clearly resolved (Figure 21), whilst microvoid coalescence is associated with the high growth rate regime (Figure 22). These features are similar to those reported by others (21-23), except that cyclic cleavage is more in evidence in the present investigation. This behaviour may result from the use of a thicker specimen combined with a waveform incorporating a tensile dwell period.

The tests restricted to minor cycles alone have used a 150-Hz sinusoidal stress wave at stress ratios of 0.74, 0.82 and 0.90. A similar test has been performed at a stress ratio approximately 0.1. In each case, crack growth measurements covering the near-threshold regime have been obtained following the determination of the threshold condition.

Yuen et al(23) have reported that Ti-6Al-4V disc material exhibits a transition from growth by cyclic cleavage to growth by a striated mechanism at a level of ΔK_{eff} of approximately 13 MPa/m. Here ΔK_{eff} is defined, not in terms of crack closure measurements as in the Elber model(14), but in the form expressed by the equation:

$$\Delta K_{eff} = \frac{1.63}{1.73-R} (\Delta K) \quad \dots (7)$$

This function effectively consolidates into a single curve the crack growth data over a wide range of positive and negative stress ratios. Based upon this criterion, all the minor cycle specimens examined have been tested within the regime giving FCG by cyclic cleavage.

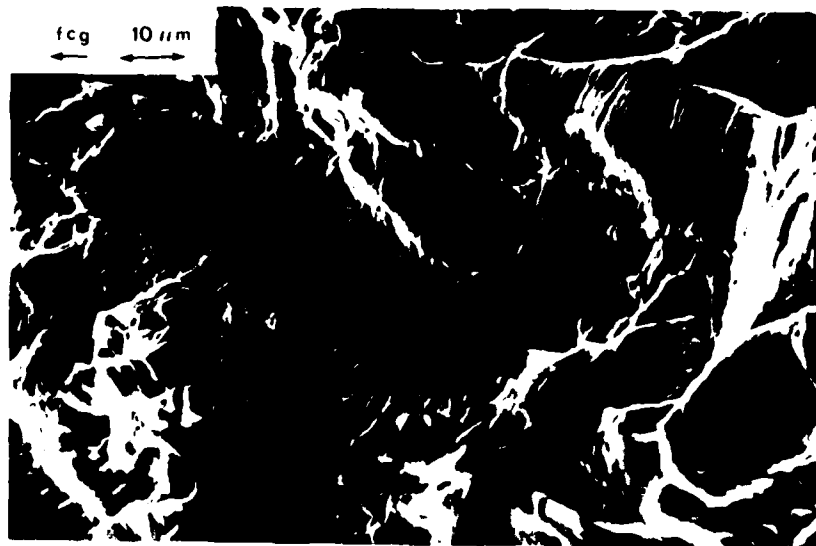


Figure 21 Large cyclic cleavage facet and region of fine ductile striations in Ti-6Al-4V generated by a major cycle loading.

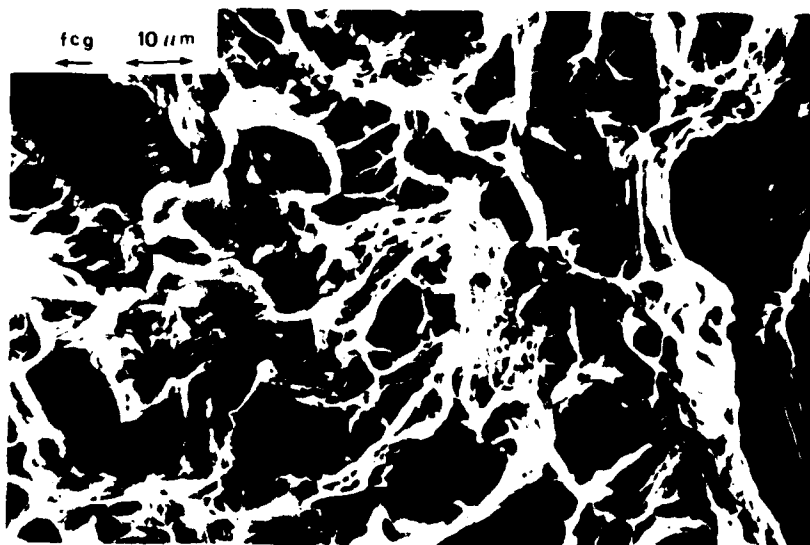


Figure 22 Major cycle growth in Ti-6Al-4V by cyclic cleavage and microvoid coalescence at $\dot{K} = 48.7 \text{ MPa}\cdot\text{m}$.

Cyclic cleavage is the predominant mode of crack growth found in all the minor cycle specimens examined (Figure 23). Having regard to the magnifications used and the prevailing growth rates, it is unlikely that any striations would be resolved. Other occasional cracking processes observed included: ductile tearing between facets, fluted or ridged regions, and transgranular facets marked with fine lines which are possibly slip band offsets. The position on each specimen corresponding to the threshold condition is not evident from the fractographic appearance. This is consistent with the observation of both Yuen et al(23) and Beevers(24) of a constant proportion of cleavage facets at stress intensities close to the threshold value. Cracking into the surface, indicative of crack tip branching, is apparent at the lowest stress intensities near to threshold and also at the final test conditions.

Experiments involving the conjoint action of major and minor stress cycles have been undertaken in two series of tests. A cycle ratio of 1000 minor cycles per major cycle combined with amplitude ratios of 0.12, 0.22 and 0.32 has been used in the first test series, and except for the early growth at the lowest amplitude ratio, the minor cycles have been active throughout.

In all cases, the FCG rate curves associated with active minor cycles are sigmoidal. For the two higher amplitude ratios, particular fatigue mechanisms may be associated with each of the three regimes of the crack growth curve. In general, the observed trend with rising ΔK is from the dominance of cleavage to the appearance initially of striated growth and eventually microvoid coalescence. The width of the striations increases with amplitude ratio. Of course, the striation markings now indicate the position of the crack front after each loading block, the markings being produced by the major load, with the crack advance due to the intervening minor cycles being unresolved. These "block striations" may display a fragmented appearance when the crack advances on parallel planes separated by surface step whose edges lie in the direction of FCG (Figure 24), whilst their width increases as the level of ΔK_{total} rises (Figure 25).

In a second series of tests, the transition from inactive to active minor cycles has been demonstrated using cycle ratios of 10,000 and 100,000 minor cycles per major cycle. Below ΔK_{onset} the fatigue cracking processes are major cycle controlled, being determined by the total stress intensity range. When ΔK_{onset} is exceeded, the minor cycle contribution to the overall growth rate increases rapidly to a level where it is dominant. Under these circumstances, the development of block striations is suppressed and the fracture surface becomes almost entirely covered by cyclic cleavage, this being the cracking process associated with minor cycle crack growth.

Longitudinal metallographic sections, prepared from selected test specimens subjected to major and minor stress cycling, have been used to identify the crack path through the Ti-6Al-4V microstructure. Crack tip branching is extensive, often beginning in a region of transformed β . The subsequent growth may include transgranular

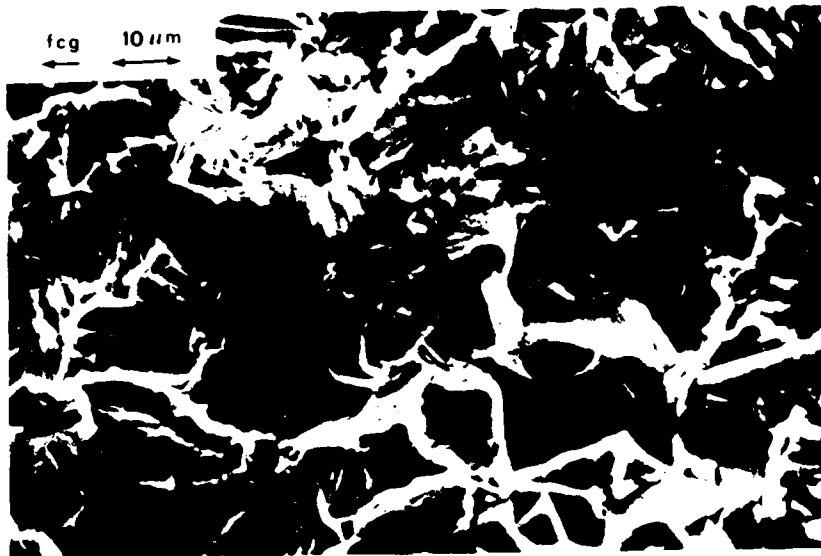


Figure 23 Minor cycle growth in Ti-6Al-4V by cyclic cleavage at a stress ratio of 0.75 and $\Delta K = 5.6 \text{ MPa}\sqrt{\text{m}}$.

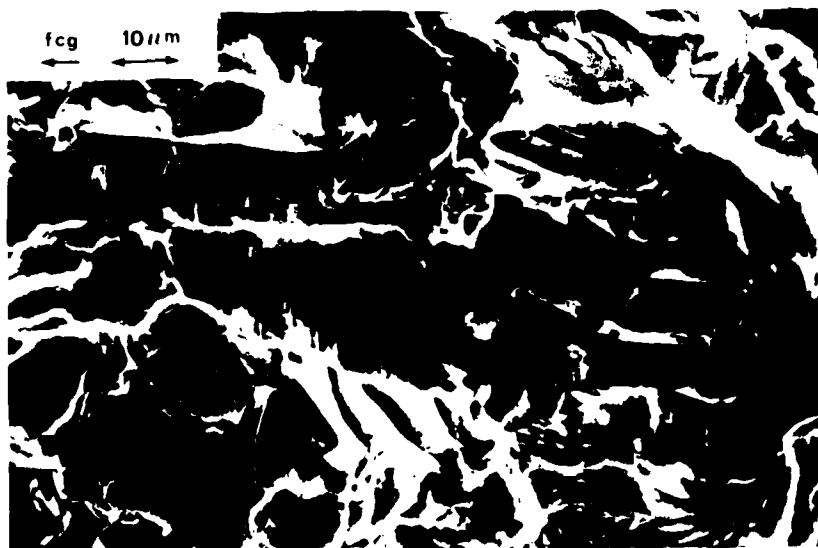


Figure 24 Cyclic cleavage and block striations resulting from major-minor cycle growth in Ti-6Al-4V, at $Q = 0.32$, $n = 1000$ and $\Delta K_{\text{total}} = 17.1 \text{ MPa}\sqrt{\text{m}}$.

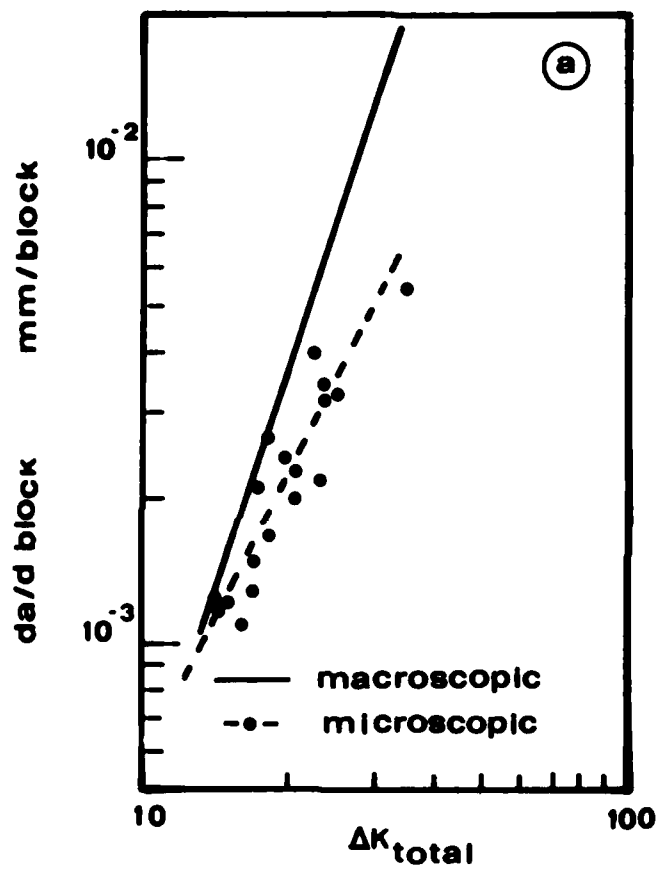


Figure 25 Comparison of macroscopic and microscopic FCG rates for Ti-6Al-4V.

fracture of the primary α , crack propagation through the transformed β sometimes crossing and sometimes running parallel to the α/β laminations, or decohesion at the primary α /transformed β boundaries. Simultaneous viewing of the metallographic section and the fracture surface, or direct etching of the fracture surface, reveals that the grains of primary α often fail by cyclic cleavage (Figure 26). Although crack growth through the transformed β laminations may produce repetitive fracture surface markings, it is clear that the block striations are unrelated to the underlying microstructure (Figure 27).

Figure 28 shows the replicated appearance of block striations as revealed by the transmission electron microscope. The surface markings produced by the major cycle appear both as crevices and protrusions, and are once more seen to be fragmented by short surface steps lying normal to the crack front. Also visible between the block striation markings are small parallel ripples (Figure 29), their number being far fewer than the 1000 minor cycles applied between major cycles.

6.3 FATIGUE CRACKING PROCESSES IN Ti-5331S

Ti-5331S can exhibit large cyclic cleavage facets because of the large grain size of the material; the fracture surface being extensively covered by cyclic cleavage within the near-threshold regime, both for separate major and minor cycle loadings. In addition, the occurrence of crack closure within a major cycle may generate fretting-oxidation debris. Striation plateaux, some with secondary cracking, are readily detected when ΔK exceeds 27 MPa \sqrt{m} ; further increases in ΔK giving greater striation spacings and the development of ductile tearing (Figure 30).

The major-minor cycle loadings applied to Ti-5331S are limited to 10,000 minor cycles per major cycle and amplitude ratios of 0.12 and 0.22. As with Ti-6Al-4V, the fracture surface topography prior to ΔK_{onset} is that associated with major cycle loadings. However, unlike Ti-6Al-4V, above ΔK_{onset} the visible evidence of minor cycle activity is the development of block striations; being detected at 26 MPa \sqrt{m} in one specimen test at $Q = 0.12$, and 17 MPa \sqrt{m} at $Q = 0.22$. Similarly, the application of a ΔK of 55 MPa \sqrt{m} is required to develop a striation spacing of 5 μm in Ti-5331S in the absence of minor cycles, whilst with superimposed minor cycles amplitudes represented by $Q = 0.12$ and 0.22, and a cycle ratio of 10 000, the required level of ΔK_{total} reduces to 33 MPa \sqrt{m} and 19 MPa \sqrt{m} respectively.

The form of block striations in Ti-5331S whilst on occasions similar to that in Ti-6Al-4V generally differs in several respects. First, at a cycle ratio of 10 000, their occurrence is extensive (Figure 31) and they grow to a spacing of 30 μm . Second, rather than being replaced by cyclic cleavage facets they are frequently superimposed on them (Figure 32). Third, those block striations having a brittle appearance possess a greater spacing than ductile striations in immediately adjacent areas (Figure 33).

Figure 34 shows the fractographic appearance of block striations commonly observed on replicas from Ti-5331S fracture surfaces. In this

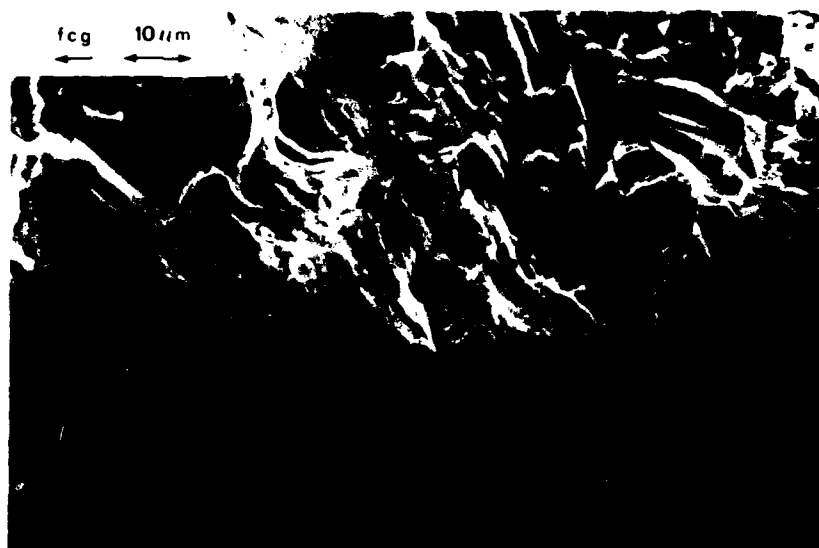


Figure 26 Longitudinal section through a Ti-6Al-4V fracture surface showing cyclic cleavage of the primary α grains and fracture surface markings associated with transformed β .



Figure 27 Longitudinal section through a Ti-6Al-4V fracture surface showing that block striations are unrelated to the underlying microstructure.



Figure 28 Transmission electron fractograph of a block striation plateau in Ti-6Al-4V. Test conditions: $Q = 0.32$ and $n = 1000$.

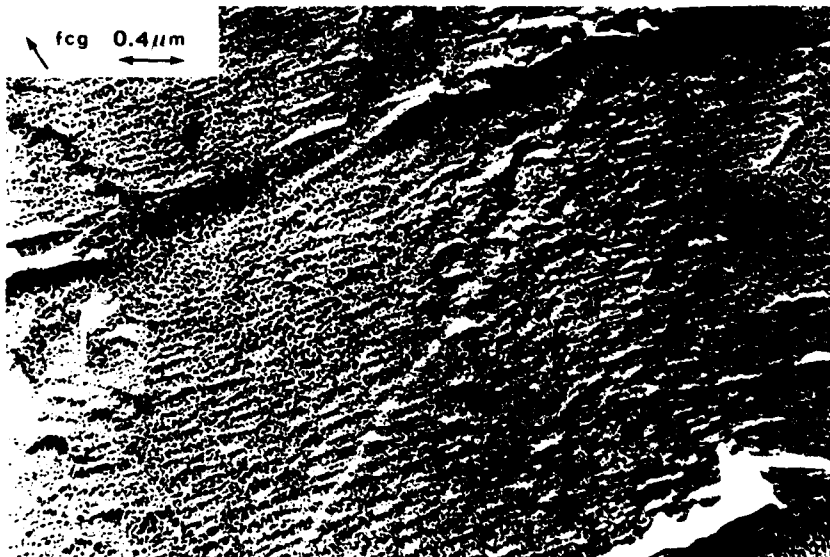


Figure 29 Transmission electron fractograph showing parallel ripple markings between block striations in Ti-6Al-4V. Test conditions: $Q = 0.32$ and $n = 1000$.

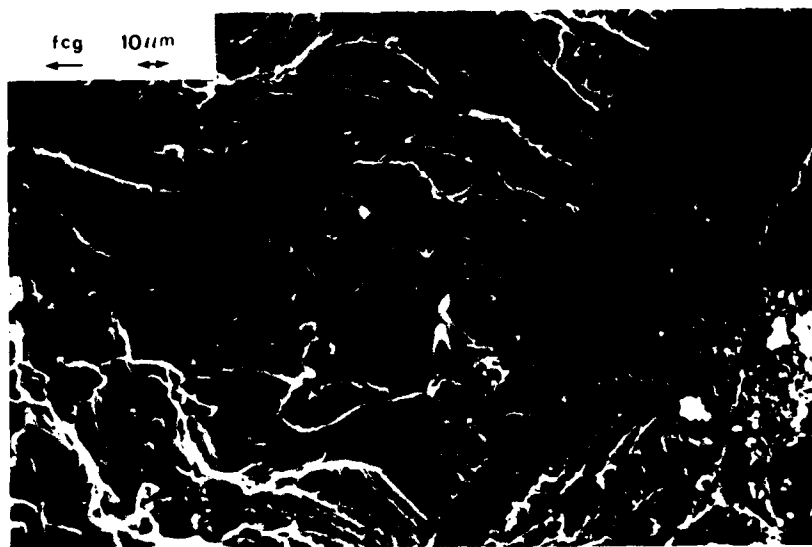


Figure 30 Major cycle growth in Ti-5331S at $\Delta K = 31 \text{ MPa}\sqrt{\text{m}}$ producing transgranular facets, striation plateaux, microvoid coalescence, and fretting-oxidation debris.

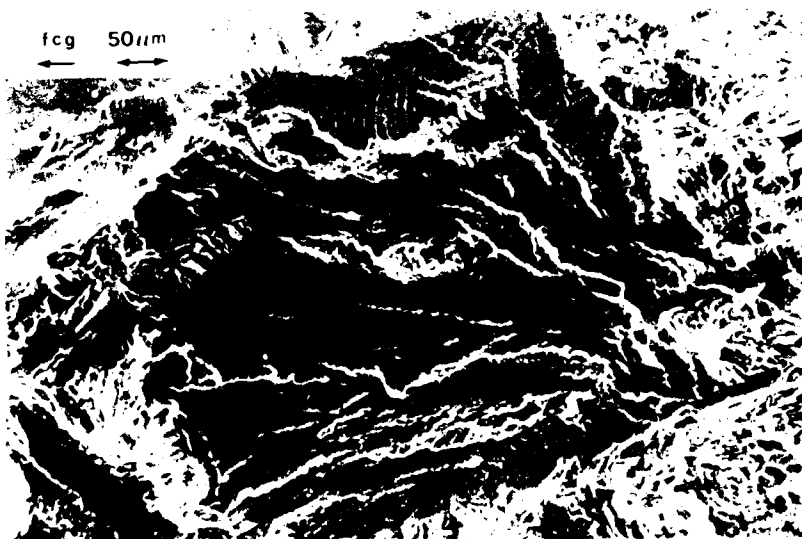


Figure 31 Division by tear ridges of a large striation plateau in Ti-5331S producing multiple, microscopic, crack front curvatures. Test conditions: $Q = 0.12$, $n = 10\,000$ and $\Delta K_{\text{total}} = 29.6 \text{ MPa}\sqrt{\text{m}}$.

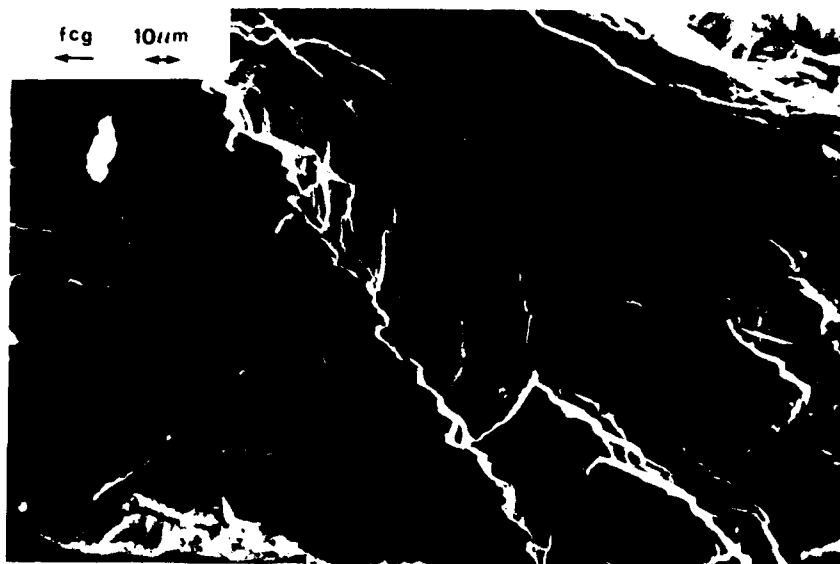


Figure 32 Curvilinear striations superimposed on a cyclic cleavage facet, and relatively straight striations on fine transverse ripple markings, developed in Ti-5331S. Test conditions: $Q = 0.22$, $n = 10\ 000$, $\Delta K_{\text{total}} = 18.2\ \text{MPa}\sqrt{\text{m}}$.

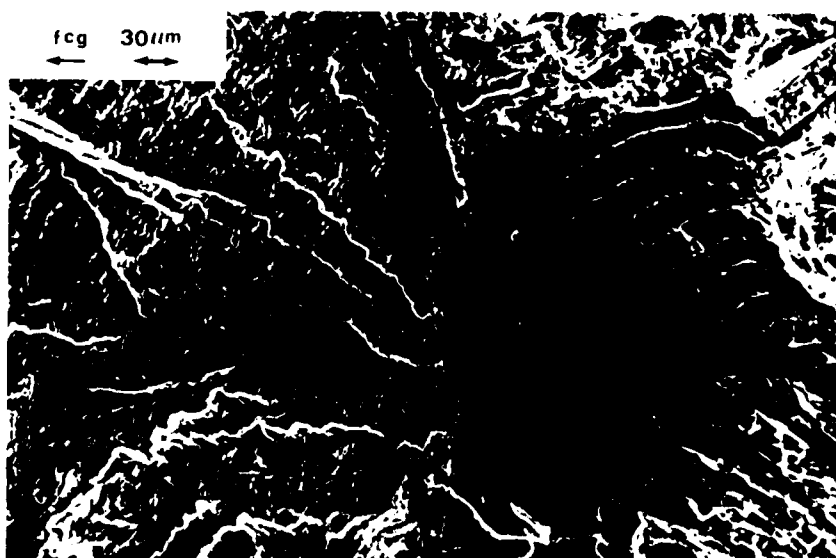


Figure 33 Large brittle striations continuous with finer ductile striations in Ti-5331S. Test conditions: $Q = 0.12$, $n = 10\ 000$, $\Delta K_{\text{total}} = 37.1\ \text{MPa}\sqrt{\text{m}}$.

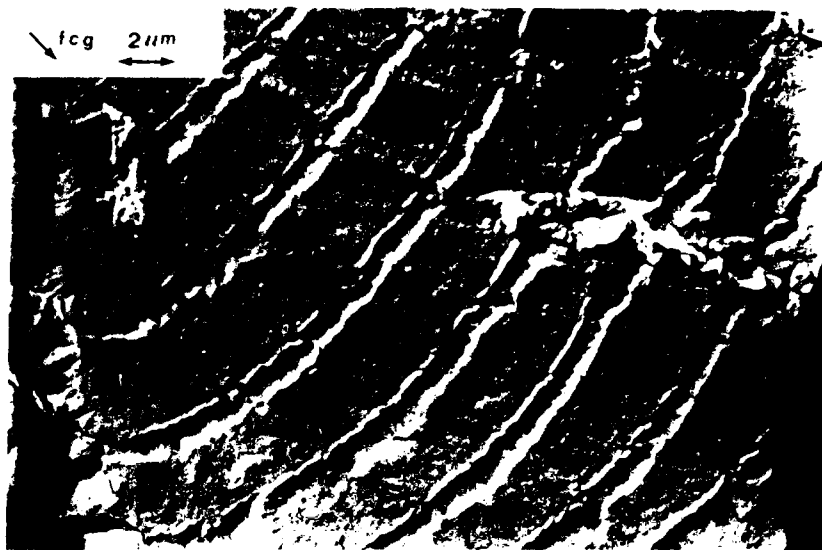


Figure 34 Transmission electron fractograph of a striation plateau in Ti-5331S. Test conditions: $Q = 0.12$ and $n = 10\,000$.

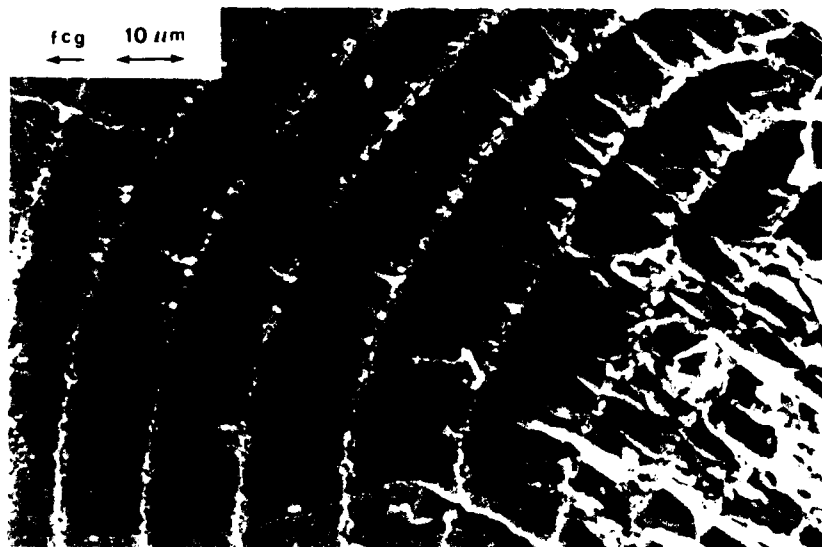


Figure 35 Brittle striations in Ti-5331S showing development of tear ridges originating at block striations which take the form of discrete and coalesced pores.

case the shadowing technique shows that the striation marking consists of a small initial lip followed by a larger rounded depression. These depressions are uneven in width and have the appearance of being formed from overlapping pores. Between the markings the fracture surface is generally featureless, although elsewhere on the same specimen parallel interstriation ripples and various tear ridges are evident (Figure 32). Figure 35 shows an enlargement of wide block striations seen in Figure 33 which have a brittle appearance. Here the block striations take the form of an irregular line of discrete pores from which many tear ridges develop.

SECTION 7

DISCUSSION

7.1 INTRODUCTION

In this chapter the results presented previously are assessed, mainly in terms of the guidance they give, both regarding the philosophy and implementation of a damage tolerance lifing policy for aeroengine discs and blades, and the crack propagation lives of such components in service.

7.2 THE ROLE OF CRACK CLOSURE

The different crack closure mechanisms which are dominant in Ti-5331S and Ti-6Al-4V must give rise to the different K_{op} versus ΔK responses observed for these two materials. Thus the higher level of K_{op} observed in Ti-5331S results from the surface roughness-induced crack closure which derives from this material's larger grain size. The extent of this closure mechanism is largely controlled by the material's microstructure, thus the level of K_{op} remains virtually constant, at least in tests which largely span the intermediate regime of FCG. This effect is much reduced in Ti-6Al-4V which exhibits a lower level of K_{op} by virtue of plasticity-induced closure. The size of the plastic zone at the crack tip will increase with ΔK , and as a consequence a progressive rise in K_{op} is to be expected.

Clearly where the crack growth is minor cycle dominated, as for example with a high Q or a combination of low Q and a high cycle ratio, the influence of any closure within the major cycle is negligible. Currently the level of vibratory stress amplitude generated within a particular gas turbine or compressor disc in service is poorly defined. As a consequence initial models describing the effects of combined major-minor cycling need not be complicated, and it is probably sufficient to correlate FCG rates above ΔK_{onset} with the applied ΔK rather than ΔK_{eff} . Similarly, a marginal reduction in FCG rates due to an extended rest period, suggested by one test, is of little practical significance. Levels of vibratory stress amplitude are crucial because they control the defect size at the onset of minor cycle activity, and hence define the end of useful life(3). The role of ΔK_{eff} is to determine the FCG rates prior to ΔK_{onset} , and thereby affect the practical lives of components subjected to a combined major-minor cycle loading.

7.3 THE ONSET OF MINOR CYCLE ACTIVITY

For components subjected to major-minor cycle loadings having a high cycle ratio, the criterion for failure is given by the fatigue threshold value associated with the minor cycles. These low amplitude stress cycles are superimposed on a high tensile mean stress, and they possess a high stress ratio, typically $R_{minor} = 0.7$ to 0.99 , as a consequence. The effect of stress ratio on the fatigue threshold stress intensity range has been the subject of considerable study(25). Essentially two forms of stress ratio dependent behaviour have been identified, the

differences being apparent at the high stress ratios which are characteristic of minor cycles.

In the first case, ΔK_{th} initially falls with an increasing stress ratio, eventually reaching a limiting value, when it remains almost unaltered despite further increases in stress ratio. This response, shown schematically in Figure 36, has been observed in some steels(26-29) and aluminium alloys(26). The concept of crack closure can be used to explain this response, as for example in the models of Schmidt and Paris (26) and Beevers(30). Each ΔK_{th} value is considered to be the sum of two terms; $\Delta K_{th i}$, the intrinsic barrier to FCG growth, and $\Delta K_{th c}$, the resistance to crack growth arising from the presence of crack closure. At high stress ratios crack closure is absent and the threshold value is constant, and equal to $\Delta K_{th i}$ (also known as $\Delta K_{th eff}$).

The accumulated data for ΔK_{th} in Ti-6Al-4V disc material(4) clearly indicates that the closure model is inappropriate. In this case, the absence of crack closure does not result in a constant level of ΔK_{th} , rather ΔK_{th} continues to decline with each increase in stress ratio. In Ti-6Al-4V the decline is essentially linear over the wide range of stress ratio investigated, but in other materials the decline at high stress ratios is more rapid(31). Whether linear or not such a continued mean stress dependence could be the result of a progressive change in FCG mechanisms. The application of a high static mean stress could modify the FCG mechanisms, perhaps by inducing a greater proportion of static fracture modes.

This second form of stress ratio dependence involving continuously declining ΔK_{th} values is also well documented. Moreover for several steels it has been demonstrated(32-36) that the effects of strength level and grain size, though significant at low stress ratios, almost disappear at high stress ratios (Figure 37).

Clearly the existence of a plateau in threshold values at high stress ratios will give a high level of ΔK_{onset} , and this suggests a greater life under combined major and minor stress cycles. What then is the form of high-R threshold behaviour displayed by near- α titanium alloys? A literature search for threshold data relating to titanium-based alloys has not revealed any high-R threshold values for near- α alloys. The most relevant information is that reported by Hicks et al(37) who have established ΔK_{th} values for Ti-65S within the range $R = 0.1$ to 0.6 . Their data was represented by a crack closure model because a constant level of $\Delta K_{th eff}$ of approximately $5 \text{ MPa } \sqrt{\text{m}}$ was observed.

The high-R threshold results now reported for Ti-5331S show that the promise of a threshold plateau in a near- α alloy is not realised. Indeed when the available results for near- α alloy are compared with those for Ti-6Al-4V the pattern is remarkably similar to that observed for many steels. Once more the effect of grain size and strength level are markedly reduced at high stress ratios (Figure 38).

Compared with Ti-6Al-4V, it is anticipated that Ti-5331S will exhibit longer fatigue crack propagation lives because of its inherently slower crack growth rates. It is evident that ΔK_{th} values associated with

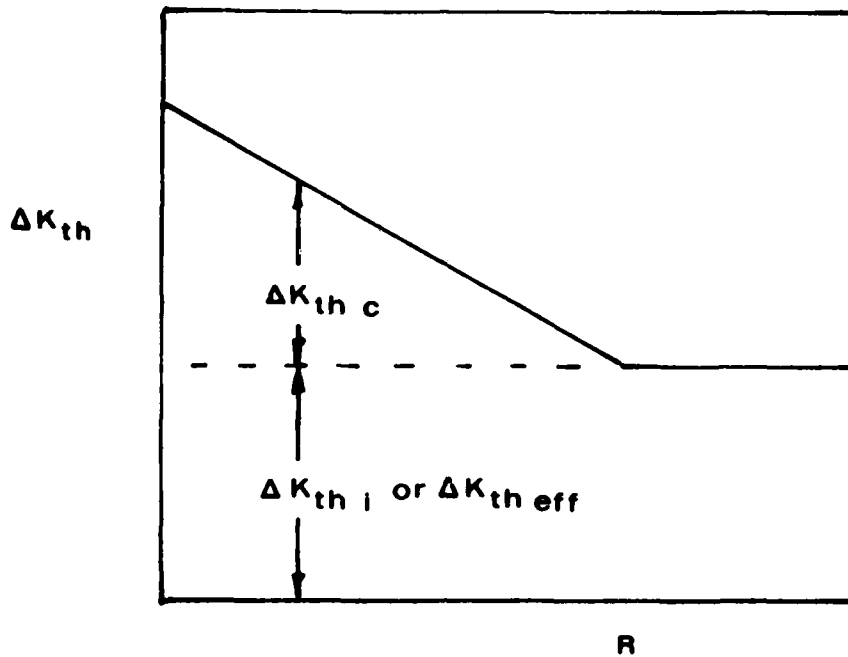


Figure 36 Dependence of fatigue threshold upon stress ratio predicted by the crack closure model.

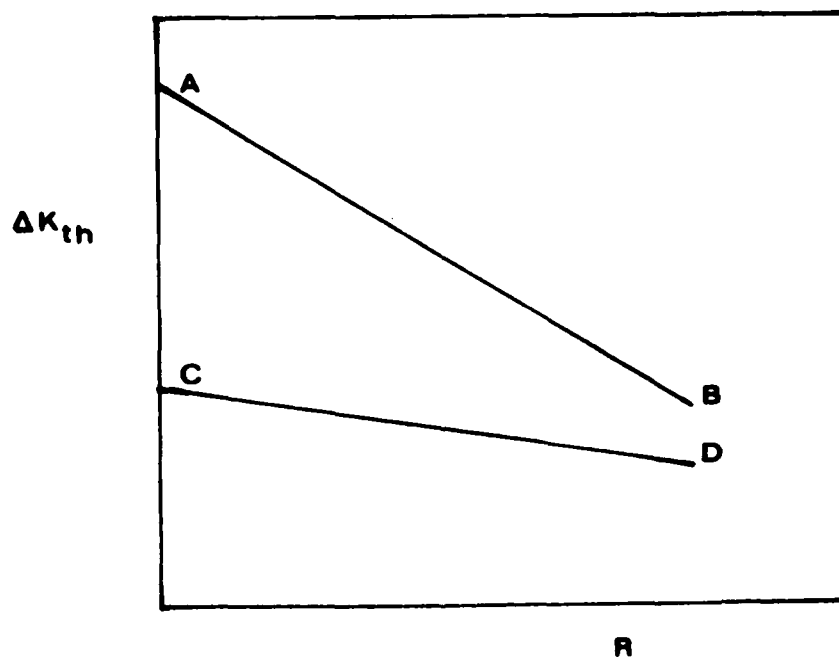


Figure 37 Continuous dependence of fatigue threshold on stress ratio. Key: AB represents the material with lower yield strength and larger grain size; CD represents the material with the high yield strength and smaller grain size.

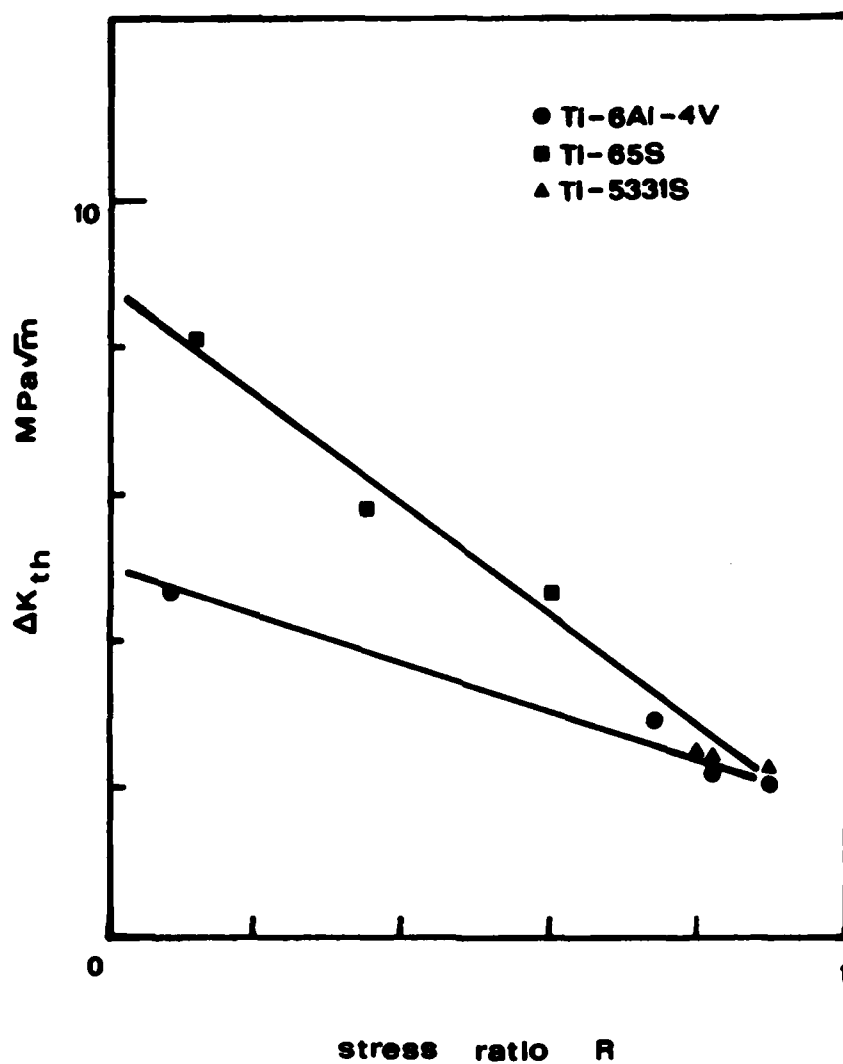


Figure 38 Variation in fatigue threshold value with stress ratio for titanium-based alloys. The near- α alloys have a prior β grain size of 0.6 mm. Data for Ti-65S from reference 37.

minor cycles of high stress ratio are likely to be of similar magnitude for $\alpha + \beta$ and near- α titanium alloys. The ΔK_{onset} values predicted for Ti-5331S are only marginally greater than those established for Ti-6Al-4V. Bearing in mind that the FCG rate will be greatest near the terminal condition, which for major-minor cycling is considered to be ΔK_{onset} , little increase in fatigue crack propagation life can be expected in Ti-5331S from this contribution. However, when assessing fatigue life for a damage tolerant design, it is the initial defect size and the early crack growth (including short crack effects), rather than the magnitude of ΔK_{onset} , which are expected to be of greatest significance.

7.4 CRACK GROWTH WITH ACTIVE MINOR CYCLES

A loading pattern of minor cycles superimposed on the dwell period of a trapezoidal major cycle can be considered as a constant amplitude loading of high stress ratio which is periodically interrupted by an underload. In a study of FCG under biharmonic loading, Fleck and Smith (38,39) have shown that periodic underloads lead to an accelerated rate of crack growth. A similar effect was reported by McMillan and Pelloux(40) for simple programme loadings having a fixed level of maximum stress. All these results are for steels and high strength aluminium alloys, and significantly they are for test conditions which combine high amplitude ratios with low cycle ratios.

The onset of minor cycle damage and the subsequent FCG rates determined experimentally exhibit slight retardation in Ti-5331S compared with the linear summation predictions. These predictions assume no effect resulting from interactions between the two levels of loading. However, the experimental results for Ti-6Al-4V are in good agreement with the predictions based on linear summation. All these tests involve low amplitude ratios and high cycle ratios as a simulation of aeroengine conditions. The applicability of linear summation predictions for these conditions is consistent with the observation that the accelerating effect of periodic underloads declines rapidly with both an increase in cycle ratio and a reduction in amplitude ratio(38,39). What is lacking is an explanation for the slight retardation found only in Ti-5331S.

The unusually blackened fracture surface observed on the specimen showing greatest retardation suggests that crack closure is involved. Few measurements of crack opening loads were taken for this particular specimen. However, it has been demonstrated that K_{op} is virtually unaffected by the addition of minor cycles, whilst crack closure has not been detected within superimposed minor cycles themselves. These observations do not support the idea that crack closure within the major cycle will influence the FCG rates which are dominated by large numbers of active minor cycles.

In his review of mechanisms of accelerated and retarded FCG, Fleck(39) has suggested several possible causes of load interaction effects. He identifies two possible contributions to accelerated FCG due to periodic unloading. First, prestrain of the material at the crack tip by the major cycle which induces a transient enhancement in the minor cycle FCG rate. Second, the restoration of the mean stress within the reversed

plastic zone by the major cycle, which subsequently decays under minor cycle growth. Both mechanisms would account for the tendency towards those growth rates predicted by linear summation at high cycle ratios. The slight retardation in FCG observed for Ti-5331S at $n = 10,000$ is more likely to be explained by the role of the major cycle in modifying such features as the sharpness of the crack tip, the material response within the plastic zone, or the mechanism of the fatigue cracking process.

7.5 FRACTURE MECHANISMS

It is clear that the addition of minor cycles to the dwell period of the major cycle can give an increase in FCG rates, and further, that this enhancement is not associated with any particular fatigue cracking process. The three regimes of the sigmoidal FCG curve, for combined major-minor cycle loading above ΔK_{onset} , cannot be related with consistency to specific cracking mechanisms, as is often the case for single-frequency loadings. Depending upon the material and levels of Q , n and ΔK_{total} , the fracture surface may exhibit, to varying degrees, a striated, faceted, or dimpled appearance. What then governs the fracture process under combined major and minor stress cycles? The dominance of either the major or the minor cycle crack growth, predicted quantitatively by the linear summation analysis, is correlated in a qualitative manner by the fracture surface morphology. Consequently, the cracking processes under combined loading may be largely anticipated from a knowledge of the cracking processes associated with the separate major and minor components.

In every specimen examined, cyclic cleavage has been involved in the fatigue cracking process to some degree. Cyclic cleavage takes the form of fan shaped facets which show little evidence of plastic deformation. The facets usually have a single point of origin from which radiate curved coarse steps called river marks (Figure 21). These indicate the direction of growth across the facet. Fine striations superimposed on the facets have been observed(23,41,42) and this has been interpreted as proof of their progressive development under cyclic loading conditions. Cyclic cleavage represents one of four possible forms of transgranular fracture of the α particles. This fracture occurs on the basal (0002) planes of the α phase, being encouraged by increasing severity of the environment, and increasing stress normal to the (0002) planes(43). In β heat treated materials large multicolony facets may form because the α platelet colonies within the same prior β grain possess a common α basal plane(44).

In general, all cleavage is induced by strain incompatibilities and two detailed mechanisms for the particular case of cyclic cleavage have been advanced. The first, proposed by Duquette and Gell(45) for stage I FCG, was applied by Yuen et al(23) to stage II crack growth. They suggested that cyclic cleavage is to be expected in Ti-6Al-4V since it is characterised by planar slip combined with a high affinity for oxygen. This absorption of oxygen at the crack tip favours crack growth since it gives a reduction in surface energy of the crack. At the same time, with planar slip there is the development of dislocation dipoles within the slip bands which intensifies the stress in the vicinity of

the slip bands. Consequently Yuen et al(23) have associated the transition from cyclic cleavage to striated growth with the transition from planar slip to multiple slip within the α particles. The critical level of ΔK_{eff} is that at which the reversed plastic zone size corresponds to the α particle size. The second mechanism, proposed by Neal and Blenkinsop(46) is an application of the Stroh mechanism for cleavage fracture(47). Dislocations pile up on prismatic planes creating a strain normal to the cleavage plane.

In Ti-6Al-4V the cyclic cleavage facets have a size which is comparable to that of the α particles, and the facets are developed over a wide range of ΔK and growth rates. At low stress intensities, macroscopic growth rates of less than one atomic spacing per cycle have been obtained for fracture surfaces which are predominately cyclic cleavage, indicating that growth by cyclic cleavage may be discontinuous. Wanhill(48) has reported that at higher levels of ΔK the transition from cyclic cleavage to striated growth may be so marked in some grades of Ti-6Al-4V that a significant change in slope of the da/dN versus ΔK curve results. However, in common with Wanhill, the results of this study indicate a gradual transition. Ward-Close and Beevers(43) have investigated the growth rates due to cyclic cleavage and fatigue striations when both are present. From a study of the macroscopic growth rates in large grained α titanium they have shown that the growth rate due to cyclic cleavage can be ten-times that associated with striated crack growth.

Under suitable conditions the application of combined major and minor stress cycles can give rise to the development of block striations. They may, therefore, be used in a failure analysis to indicate the application in service of such a loading. This must be done with caution since similar features can be observed under single-frequency loading. Smooth transgranular facets may be divided by well spaced parallel lines whose origins are probably that of slip band offsets, whilst in transformed β , cleavage facets can display small white relief markings where the facet crosses a succession of platelet interfaces (49). The greatest doubt arise from crack propagation through a laminated structure, where there is a possibility of secondary microcracks developing at each of the parallel platelet interfaces(49). Why then are the observed repetitive surface markings identified as block striations? In the first instance, they often possess the curvilinear shape characteristic of fatigue striations. Also, they are observed in a wide range of materials, including a high strength aluminium alloy (RR58) and a nickel-based superalloy (Waspaloy) which possess no laminated two-phase microstructure(50). Even in Ti-6Al-4V, there is no correlation between the orientation and spacing of the block striations on the fracture surface and the disposition of platelets in the underlying microstructure (Figure 27). Finally and convincingly, their width increases with crack length and thus with ΔK , giving growth rates similar to those measured macroscopically (Figure 25).

Where such relationships are established for a wide range of engine operational conditions, it is possible that the measurement of block striation widths might be used quantitatively in a failure analysis. In Waspaloy, for example, the fracture surface may be extensively covered

by block striations, and as a consequence, their width correlates well with the measured macroscopic growth rates(50). In the case of a failed aeroengine component fabricated from such a material, the width of the block striations might be used to estimate the amplitude ratio, given that a value of cycle ratio could be assumed from a vibrational analysis of the component and a knowledge of the past engine missions. This estimate would be of value because there is considerable uncertainty regarding the magnitude of vibrations in individual blades and discs when in service. Whether this form of analysis could be applied to components of Ti-6Al-4V is doubtful, for two reasons. First, block striations were largely absent at high cycle ratios, and second, those block striations developed at a low cycle ratio gave an underestimation of the macroscopic growth rates (Figure 25). The latter is a well documented effect(51-56), occurring in this instance because much of the growth is by the faster process of cyclic cleavage.

The process of beach marking a fracture surface by a periodic shift in the stress ratio of the applied loading has frequently been used both to calibrate crack length measuring systems and to define the changing shape of a developing crack(57-59). The periodic changes in loading visibly mark the fracture surface due to systematic changes in the surface texture. Forsyth(59,60) has shown that a biharmonic loading, consisting of a constant amplitude stress wave superimposed upon a periodically varying mean stress, can similarly mark successive positions of the crack front on the microscopic level. In this case, the growth at low stress ratios may be significantly retarded relative to constant amplitude FCG rates. The major-minor cycle loading patterns used in the present test programme can similarly mark the fracture surface with block striations, with little or no crack growth retardation.

The unloading at the major cycle, marks, with a single striation, the crack advance produced by the intervening minor cycles of high stress ratio. Thus, the progressive development of a cyclic cleavage facet during FCG is clearly demonstrated by the superimposed block striations, for they appear as regularly spaced concentric markings which develop from the origin of the facet (Figure 32). Similarly, Figure 31 shows the development of independent, microscopic, crack front curvatures. As proposed by Forsyth(59), each set of striations has a radius of curvature which is approximately equal to the striation plateau width.

Several investigators(61-63) have examined the striated appearance of aluminium alloys subjected to a simple repeated loading block. In every case, this consisted of 10 cycles at $R = 0.5$ and 1 cycle at $R = 0$ with the same maximum stress. The ΔK associated with the smaller stress cycles was such that 10 distinct striations were observed between the larger individual striations. Given the similarity of loading pattern used in the present study, is it possible that individual minor cycle striations might be resolved between the block striations? Certainly fine markings parallel to the block striations are apparent on several electron fractographs, but the number of such marking is far less than the number of minor cycles involved. Indeed, it is not expected that the test conditions, involving low amplitude ratios combined with high cycle ratios, will generate visible minor cycle striations. The use of 10 000 minor cycles per major cycle in the development of block striation

widths of 1-30 μm implies an average minor cycle growth rate of approximately 0.1-30 nm/cycle. These crack growth increments are below the limit of detection for fatigue striations(64-66), and sometimes less than 1 atomic spacing. The fine markings observed between block striations are therefore considered to be evidence of the accumulation of deformation and fracture processes associated with minor cycle crack growth.

Block striations were not observed on cyclic cleavage facets in Ti-6Al-4V. Using the technique of electron channelling patterns, Ward-Close and Beevers(43) have shown that the fracture mode in α titanium is dependent upon the orientation of each grain relative to the maximum tensile loading axis. Cyclic cleavage occurs on the (0002) basal plane when the basal pole lies within 60° of the tensile axis, the incidence of cleavage fracture depending on the level of stress intensity range and environment. Striations are, by contrast, formed on planes normal to the (0002) basal plane with the striation front parallel to the [0001] crystal direction. Striations will form where the c-axis of a close packed hexagonal unit cell is more than 75° from the tensile axis and more than 50° from the macroscopic FCG direction. These observations, which may be summarised in a grain orientation control map(129), show that in α titanium cyclic cleavage and striated growth are mutually exclusive.

The fracture path in β heat-treated titanium alloys again results from a compromise between the influence of mechanical factors, such as local stress state, and microstructural features which control the energy consumed in crack propagation. Although relatively ductile separation occurs along α platelet interfaces or at α colony boundaries, cyclic cleavage and a brittle fracture appearance results from the preferred crystallographic growth across α platelets(49). In β processed Ti-65S having a basketweave microstructure, the effect of applying an extended dwell period on maximum load is to increase the occurrence of cyclic cleavage, whilst creating regions of brittle striations which have a greater spacing than the adjacent ductile variety(67). These effects may be attributed to the precipitation of hydrides on the basal plane of the titanium crystal lattice. Forsyth(58) suggests that there is little intrinsic difference between the mechanisms of ductile and brittle striation formation; and that the difference in appearance derives from the greater width of the brittle striations, these occurring in association with crystal orientations having easy crack paths. Figure 33 shows the presence in Ti-5331S of adjacent brittle and ductile block striations which are probably associated with grains or α colonies having different orientations.

Although the presence of block striation markings clearly defines the cyclic development of pseudo-cleavage facets, it may also modify the fracture surface morphology and growth kinetics. Figures 32 and 35 show that the periodic marking of the surface by the major cycle initiates many steps or tear ridges, perhaps as a consequence of either crack tip blunting or branching. Thus, there is an increase in the total length of the crack, which now advances on a greater number of parallel cleavage planes, with the energy absorbing process of ductile

tearing occurring between these sections. As the crack grows, the number and size of the ridges declines but is re-established at the next major cycle. Thus, the retardation in FCG rates relative to the predictions of linear summation, observed for Ti-5331S, may arise in part from the interaction between cyclic cleavage and striated crack growth.

7.6 CONCLUDING REMARKS

The engineering significance of the results presented relates to the *implementation of a policy of retirement for cause for aeroengine discs and blades*. It has been shown that the condition defining the end of the useful life of such components can be safely predicted from a knowledge of minor cycle threshold values. There is now a clear need to test the validity of this design rule for the frequently observed corner crack configuration, including cracks of limited size in which short crack effects are to be found. Further testing involving elevated temperatures is required in order to describe the minor cycle activity under conditions which more closely simulate engine operations.

SECTION 8

CONCLUSIONS

1. Fatigue crack growth rates in the near- α titanium alloy Ti-5331S have been determined using a trapezoidal major cycle loading. These results are in agreement with published data for this material. The different major cycle growth rates observed for Ti-6Al-4V and Ti-5331S are reconciled by the use of an effective range of stress intensity.
2. At stress ratios of 0.8 to 0.9 the fatigue threshold values established for Ti-5331S are in the range 2.5 to 2.3 MPa \sqrt{m} . These results demonstrate that threshold values in a near- α titanium alloy cannot be predicted by an effective threshold concept. A mean stress effect is apparent at high stress ratios, characteristic of minor cycle loadings, where closure is absent.
3. The addition of minor cycles to the dwell period of the major cycle does not change the crack opening behaviour associated with the major cycle. When the advance of a fatigue crack is used to generate a progressive increase in the stress intensity range applied to a compact tension testpiece, the bulk measurement of crack opening stress intensity remains almost constant in Ti-5331S, but rises linearly in Ti-6Al-4V.
4. Under combined major-minor cycle loadings possessing a high cycle ratio, the useful life of a component is defined by the onset of minor cycle crack growth. The relative fatigue threshold values, for high tensile mean stresses, show that the resistance of Ti-5331S to minor cycle crack growth is only marginally greater than that of Ti-6Al-4V. It is because of its slower major cycle growth rates, and not because of any significant delay in minor cycle crack growth, that Ti-5331S can be expected to show greater fatigue crack propagation lives under combined major-minor cycle loadings.
5. The onset of minor cycle activity under combined major and minor cycle loading has been demonstrated for long through cracks in Ti-6Al-4V. Using cycle ratios of 10 000 and 100 000 minor cycles per major cycle and amplitude ratios of 0.06, 0.12, 0.22 and 0.32, good correlation has been obtained between the total stress intensity range corresponding to the onset of minor cycle activity and the fatigue threshold value for the minor cycles. For long through cracks in Ti-5331S this correlation gives either an accurate or safe prediction of the useful life of rotating aeroengine components, because they experience high frequency vibrations in large numbers.
6. Following the onset of minor cycle damage, the FCG rates in Ti-6Al-4V for combined major and minor cycling involving 1000 to 100.000 minors per dwell periods, are predicted by the linear summation of the major and minor cycle contributions to crack growth. In Ti-5331S, the linear summation of crack growth associated with the

low and high cycle fatigue loadings gives either an accurate or safe prediction of the observed crack growth rates.

7. Exploratory tests suggest that a 50-fold increase in the major cycle rest period produces a marginal reduction in fatigue crack propagation rates.
8. Major cycle loadings produce a succession of largely faceted, striated, and dimpled fracture surfaces and progressively higher stress intensity ranges. The minor cycle crack growth is dominated by the formation of cyclic cleavage facets.
9. Prior to the onset of minor cycle activity, the fatigue cracking processes are those associated with major cycle crack growth. Subsequently, the minor cycle crack growth may generate extensive cyclic cleavage or increase the separation of fatigue striations associated with the periodic major cycles. The operation of combined major and minor stress cycles may be diagnosed from the observation of these extended striations, and where they extensively cover the fracture surface, they may be used to estimate the average crack advance per minor cycle.

REFERENCES

1. Annis, C.G. Jr., Van Wanderham, M.C., Harris, J.A. Jr., and Sims, D.L. "Gas turbine engine disk retirement-for-cause: an application of fracture mechanics and NDE", *Trans. ASME, J. Engrg. for Power*, 1981, 103, 198-200.
2. Duggan, T.V. "Low cycle failure mechanisms", *Engrg. Mater and Design*, 1972, 16, 24-28.
3. Powell, B.E., Duggan, T.V. and Jeal, R.H. "The influence of minor cycles on low cycle fatigue crack growth", *Int. J. of Fatigue*, 1982, 4, 4-14.
4. Powell, B.E. and Henderson, I. "The conjoint action of high and low cycle fatigue", *AFWAL-TR-83-4119*, Air Force Wright Aeronautical Laboratories, Wright-Patterson Air Force Base, Ohio, November 1983.
5. Powell, B.E., Henderson, I. and Duggan, T.V. "The effect of combined major and minor stress cycles on fatigue crack growth", *2nd Int. Conf. on Fatigue and Fatigue Thresholds*, Birmingham, 1984, 2, 893-902.
6. Roberts, D.R.T. "A machine for testing material", *UK Patent Application GB 2 081 457 A*, London, 17th February 1982.
7. ASTM "Tentative test method for constant amplitude fatigue crack growth above 10^{-8} m/cycle - ASTM standard E 647-83", *ASTM Book of Standards*, ASTM, Philadelphia, 1983, Part 3, 710-730.
8. Driver, D., Hall, D.W. and Meetham, G. "The gas turbine engine", *The Development of Gas Turbine Materials*, Ed. Meetham, G.W., Applied Science, London, 1981.
9. Halliday, M.D. and Beevers, C.J. "Some aspects of fatigue crack closure in two contrasting titanium alloys", *J. of Testing and Evaluation*, 1981, 9, 195-201.
10. Morton, P.H. "Titanium alloys for engineering structures", *Phil. Trans. R. Soc.*, 1976, 282, 401-411.
11. Duncan, R.M., Goosey, R.E., Jeal, R.H. and Postans, P.J. "Process development and evaluation of gas turbine engine components in IMI 829", *4th Int. Conf. on Titanium - Titanium '80 Science and Technology*, Met. Soc. AIME, New York, 429-439.
12. Hicks, M.A. "Slow fatigue crack growth and threshold behaviour in IMI 685", *Ph.D. Thesis*, University of Birmingham, 1980.
13. Elber, W. "Fatigue crack closure under cyclic tension", *Engrg. Fracture Mech.*, 1970, 2, 37-45.

14. Elber, W. "The significance of fatigue crack closure", *Damage Tolerance in Aircraft Structures - ASTM STP 486*, ASTM, Philadelphia, 1971, 230-242.
15. Halliday, M.D. and Beevers, C.J. "Non-closure of cracks and fatigue crack growth in β heat treated Ti-6Al-4V", *Int. J. of Fracture*, 1979, 15, R27-R30.
16. Walker, N.J. and Beevers, C.J. "A fatigue crack closure mechanism in titanium", *Fatigue of Engrg. Mats. and Structures*, 1979, 1, 135-148.
17. Byrne, J. "Fatigue resistance in alloys - influence of crack closure and geometry on fatigue thresholds", *Ph.D. Thesis*, Portsmouth Polytechnic, October 1981.
18. Scheffel, R. and Detert, K. "The influence of crack closure on the fatigue crack propagation in the aluminium alloy Al Mg Si 1", *Life Assessment of Dynamically Loaded Materials and Structures, 5th European Conf. on Fractures*, Lisbon, 1984, 2, 805-814.
19. Kikukawa, M., Jono, M. and Tanaka, K. "Fatigue crack closure behaviour at low stress intensity level", *Proc. 2nd Int. Conf. on Mechanical Behaviour of Materials*, Boston, 1976, 254.
20. Gauthier, P., de Rabaudy, H. and Auvinet, J. "Secondary cracking processes during fatigue crack propagation", *Engrg. Fracture Mech.*, 1973, 5, 977-981.
21. Hertzberg, R.W. and Mills, W.J. "Character of fatigue fracture micromorphology in the ultra-low growth rate regime", *Fractography-Microscopic Cracking Processes, ASTM STP 600*, ASTM, Philadelphia, 1976, 220-234.
22. Bucci, R.J., Paris, P.C., Hertzberg, R.W., Schmidt, R.A. and Anderson, A.F. "Fatigue threshold crack propagation in air and dry argon for a Ti-6Al-4V alloy", *Stress Analysis and Growth of Cracks, ASTM STP 513*, ASTM, Philadelphia, 1972, 125-140.
23. Yuen, A., Hopkins, S.W., Leverant, G.R. and Rau, C.A. "Correlations between fracture surface appearance and fracture mechanics parameters for stage II fatigue crack propagation in Ti-6Al-4V", *Met. Trans.*, 1974, 5A, 1833-1842.
24. Beevers, C.J. "Fatigue crack growth characteristics at low stress intensities in metals and alloys", *Metal Sci.*, 1977, 11, 362-367.
25. Byrne, J., Duggan, T.V. and Beevers, C.J. "Crack closure and the stress ratio dependence of the fatigue threshold stress intensity range", *Technical Report F389*, Portsmouth Polytechnic, March 1985.
26. Schmidt, R.A. and Paris, P.C. "Threshold for fatigue crack propagation and effects of load ratio and frequency", *Progress in*

Flaw Growth and Fracture Toughness Testing - ASTM STP 536, ASTM, Philadelphia, 1973, 79-94.

27. Paris, P.C., Bucci, R.J., Wessel, E.T., Clarke, W.G. and Mayer, T.R. "Extensive study of low fatigue crack growth rates in A533 and A508 steels", *Stress Analysis and Growth of Cracks - ASTM STP 513*, ASTM, Philadelphia, 1972, 141-176.
28. Ritchie, R.O., Suresh, S. and Moss, C.M. "Near-threshold fatigue crack growth in 2½ Cr-1 Mo pressure vessel steel in air and hydrogen", *Trans. ASME - J. of Engrg. Mats. and Technol.*, 1980, 102, 293-299.
29. Suresh, S. and Ritchie, R.O. "On the influence of environment on the load ratio dependence of fatigue thresholds in pressure vessel steel", *Engrg. Fracture Mech.*, 1983, 18, 785-800.
30. Beevers, C.J. "Some aspects of the influence of microstructure and environment of ΔK thresholds", *Fatigue Thresholds-Fundamentals and Engineering Applications*, Ed. C.J. Beevers, EMAS, Warley, UK, 1981, 1, 257-273.
31. Branco, C.M., Radon, J.C. and Culver, L.E. "Growth of fatigue cracks in steels", *Metal Sci.*, 1976, 10, 147-155.
32. Gray, G.T., Thompson, A.W., Williams, J.C. and Stone, D.H. "Influence of microstructure on fatigue crack growth behaviour in fully pearlitic steels", *Fatigue Thresholds - Fundamentals and Engineering Applications*, EMAS, Warley, UK., 1981, 1, 345-361.
33. Stewart, A.T. "The influence of environment and stress ratio on fatigue crack growth at near-threshold stress intensities in low-alloy steels", *Engrg. Fracture Mech.*, 1980, 13, 463-470.
34. Ritchie, R.O. "Near-threshold fatigue-crack propagation in steels", *Int. Met. Rev.*, 1975, 24, 205-230.
35. Ritchie, R.O. and Suresh, S. "Some consideration of fatigue crack closure at near-threshold stress intensities due to fracture surface morphology", *Met. Trans.*, 1982, 13A, 937-940.
36. Druce, S.G. "Fatigue of ferritic steels", PhD. Thesis, University of Birmingham, quoted by Davidson, D.L. "Incorporating thresholds and environmental effects into the damage accumulation model for fatigue crack growth", *Fatigue Engrg. Mats. and Struts.*, 1981, 3, 227-236.
37. Hicks, M.A., Jeal, R.H. and Beevers, C.J. "Slow fatigue crack growth and threshold behaviour in IMI 685", *Fatigue Engrg. Mats. Struts.*, 1983, 6, 51-65.
38. Fleck, N.A. and Smith, R.A. "Accelerated fatigue crack growth in a low strength steel", *Digital Techniques in Fatigue*, Ed. B.J. Dabell, Soc. of Environmental Engrs., London, 1983, 190-196.

39. Fleck, N.A. "Mechanisms of accelerated fatigue growth", Submitted to *Acta Met.*
40. McMillan, J.C. and Pelloux, R.M.N. "Fatigue crack propagation under program and random loads", *Fatigue Crack Propagation - ASTM STP 415*, ASTM, Philadelphia, 1967, 505-535.
41. Yoder, G.R., Cooley, L.A. and Crooker, T.W. "Observations on microstructurally sensitive fatigue crack growth in a Widmanstatten Ti-6Al-4V alloy", *Met. Trans.*, 1977, 8A, 1737-1743.
42. Meyn, D.A. "An analysis of frequency and amplitude effects on corrosion fatigue crack propagation in Ti-8Al-1Mo-1V", *Met. Trans.*, 1971, 2A, 1325-1331.
43. Ward-Close, P.E. and Beevers, C.J. "The influence of grain orientation on the mode and rate of fatigue crack growth in α -titanium", *Met. Trans.*, 1980, 11A, 1007-1017.
44. Eylon, D. "Faceted fracture in beta annealed titanium alloys", *Met. Trans.*, 1979, 10A, 311-317.
45. Duquette, D.L. and Gell, M. "The effect of environment on the mechanism of stage I fatigue fracture", *Met. Trans.*, 1971, 2A, 1325-1331.
46. Neal, D.F. and Blenkinsop, P.A. "Internal fatigue origins in α - β titanium alloys", *Acta Met.*, 1976, 24, 57-63.
47. Smallman, R.E. *Modern Physical Metallurgy*, 3rd Ed., Butterworths, London, 1970, 465-467.
48. Wanhill, R.J.H. "Environmental fatigue crack propagation in Ti-6Al-4V", *Met. Trans.*, 1976, 7A, 1365-1373.
49. Lehr, P. "Microscopic features of fractures and crack propagation of titanium alloys", *4th Int. Conf. on Titanium, Titanium '80 Science and Technology*, Met. Soc. AIME, New York, 1980, 1617-1626.
50. Powell, B.E. "The influence of minor cycles on low cycle fatigue crack growth", *PhD. Thesis*, Portsmouth Polytechnic, 1985.
51. Miller, G.A. "Fatigue fracture appearance and the kinetics of striation formation in some high-strength steels", *Trans. ASM.*, 1969, 62, 651-658.
52. Kershaw, J. and Liu, H.W., "Electron fractography and fatigue crack propagation in 7075-T6 aluminium sheet", *Int. J. Fracture*, 1971, 7, 269-276.
53. Heiser, F. and Hertzberg, R.W. "Anisotropy of fatigue crack propagation", *Trans. ASME, J. Basic Engrg.*, 1971, 93, 211-217.

54. Broek, D. "The effect of intermetallic particles on fatigue crack propagation in aluminium alloys", *2nd Int. Conf. on Fracture*, Brighton, 1969, 754-764.
55. Bates, R.C., Clark Jr., W.G. and Moon, D.W. "Correlation of fractographic features with fracture mechanics data", *Scientific Paper 68-LD4-FRACY-PL*, Westinghouse Research Laboratories, April 1968.
56. Pelloux, R.M.N. "Fractographic analysis of the influence of constituent particles on fatigue crack propagation in aluminium alloys", *Trans ASM*, 1964, 57, 511-518.
57. Pickard, A.C. and Hicks, M.A. "Crack length determination using the d.c. electrical p.d. technique - a comparison of calibration methods", *Advances in Crack Length Measurement*, EMAS, Warley, 1982, 97-113.
58. Forsyth, P.J.E. "The growing fatigue crack in the aircraft environment", *Fatigue 84, 2nd Int. Conf. on Fatigue and Fatigue Threshold*, Birmingham, 1984, 2, 637-647.
59. Forsyth, P.J.E. "A unified description of micro and macroscopic fatigue crack behaviour", *Technical Report 82065*, Royal Aircraft Establishment, Farnborough, 1982.
60. Forsyth, P.J.E. "The determination of fatigue crack history from fracture surface analysis", *Advances in Crack Length Measurement*, EMAS, Warley, 1982, 3-40.
61. Laird, C. and de la Veaux, R. "Additional evidence for the plastic blunting process of fatigue crack propagation", *Met. Trans.*, 1977, 8A, 657-664.
62. Wanhill, R.J.H. "Fractography of fatigue crack propagation in 2024-T3 and 7075-T6 aluminium alloys in air and vacuum", *Met. Trans.*, 1975, 6A, 1587-1596.
63. Schijve, J. "Significance of fatigue cracks in micro-range and macro-range", *Fatigue Crack Propagation, ASTM STP 415*, ASTM, Philadelphia, 1967, 415-459.
64. Schijve, J and de Rijk, P. "The effect of ground-to-air cycles on the fatigue crack propagation in alclad sheet material", *NLR-TR-M 2138*, Nat. Aerospace Laboratories, Amsterdam, July 1965.
65. Christensen, R.H. "Cracking and fracture in metals and structures", *Crack Propagation Symp.*, Cranfield, 1961, 2, 326.
66. Hertzberg, R.W. "Application of electron fractography and fracture mechanics to fatigue crack propagation", *PhD. Thesis*, Lehigh University, Bethlehem, May 1965.

67. Postans, P.J. and Jeal, R.H. "Dependence of crack growth performance upon structure in β processed titanium alloys", *Forging and Properties of Aerospace Materials*, The Metals Soc., London, 1978, 192-198.

LIST OF SYMBOLS AND ABBREVIATIONS

$K_{\text{major max}}$	maximum stress intensity associated with the applied trapezoidal major cycle (MPa $\sqrt{\text{m}}$).
K_{min}	minimum stress intensity (MPa $\sqrt{\text{m}}$).
K_{op}	crack opening stress intensity (MPa $\sqrt{\text{m}}$).
P_{max}	maximum load (N).
P_{min}	minimum load (N).
P_{op}	crack opening load (N).
Q	ratio of minor cycle amplitude to major cycle amplitude.
R	stress ratio.
R_{major}	stress ratio for the applied major cycle.
R_{minor}	stress ratio for the superimposed minor cycles.
U	crack opening ratio.
$\frac{da}{d \text{ block}}$	crack growth per major-minor loading block (mm/block).
$\frac{da}{dN}$	crack growth per cycle (mm/cycle).
n	number of minor cycles per major cycle.
ΔK	stress intensity range (MPa $\sqrt{\text{m}}$).
ΔK_{eff}	effective stress intensity range (MPa $\sqrt{\text{m}}$).
ΔK_{major}	stress intensity range associated with the applied major cycle (MPa $\sqrt{\text{m}}$).
ΔK_{minor}	stress intensity range associated with superimposed minor cycles (MPa $\sqrt{\text{m}}$).
ΔK_{onset}	value of ΔK_{total} corresponding to the onset of minor cycle damage (MPa $\sqrt{\text{m}}$).
ΔK_{th}	fatigue threshold value (MPa $\sqrt{\text{m}}$).
$\overline{\Delta K}_{\text{th}}$	value of ΔK_{th} minor indicated by a linear regression model of threshold versus stress ratio data (MPa $\sqrt{\text{m}}$).
$\Delta K_{\text{th c}}$	resistance to fatigue crack growth arising from crack

LIST OF SYMBOLS AND ABBREVIATIONS (CONTINUED)

	closure.
$\Delta K_{th \text{ eff}}$	closure-free component of ΔK_{th} .
$\Delta K_{th \text{ i}}$	intrinsic resistance of a material to fatigue crack growth.
$\Delta K_{th \text{ minor}}$	fatigue threshold value corresponding to a given minor cycle stress ratio (MPa \sqrt{m}).
ΔK_{total}	stress intensity range associated with the total, or overall, stress cycle (MPa \sqrt{m}).
BFS	back face strain.
CT	compact tension.
DCPD	direct current potential difference.
FCG	fatigue crack growth.
HCF	high cycle fatigue.
LCF	low cycle fatigue.